NASA
Technical
Paper
2312

May 1984

Fracture Toughness and Flaw Growth in Nitronic 40 at Cryogenic Temperatures

Marcia S. Domack

NASA

NASA Technical Paper 2312

1984

Fracture Toughness and Flaw Growth in Nitronic 40 at Cryogenic Temperatures

Marcia S. Domack

Langley Research Center
Hampton, Virginia

NASA
National Aeronautics
and Space Administration

Scientific and Technical Information Branch

INTRODUCTION

Advances in aeronautical research and technology have led to the use of gaseous airflow at cryogenic temperatures to explore high Reynolds number conditions in the transonic flight regime. This technique has created new challenges for development of and design with new wind-tunnel model materials requiring combinations of extremely high strength and toughness. Initial design criteria (ref. 1) for cryogenic wind-tunnel models have required a combination of properties that few materials can provide. Identification and review of the small number of materials having the potential to approach design property requirements have revealed the inadequacy of mechanical property data in the temperature range of interest. Material selections were made with the condition that the unavailable property information would be obtained and used to define allowable wind-tunnel operating envelopes. One such material is Armco Nitronic 40 stainless steel, an austenitic stainless steel strengthened with the addition of 0.3 percent nitrogen, which has been selected for fabrication of the wing of the Pathfinder I model. This model is to be tested in the National Transonic Facility (NTF), located at the Langley Research Center (LaRC). The selection of Nitronic 40 was based on favorable producer-reported material properties (ref. 2), but fracture resistance information on this alloy was considered inadequate.

The NTF operates at high dynamic pressures and cryogenic temperatures in order to achieve high Reynolds number flight conditions. (See ref. 3.) The severe operating envelope of the NTF results in complex thermal and mechanical loading of models, stings, and balances. At very low temperatures, strength of structural metallics is usually increased but fracture toughness is typically reduced. Very high fracture toughness has been identified as a design requirement in order to accommodate the many geometric features which act as stress concentrators on a typical model. High fatigue strength and low crack growth rates are also necessary properties for material application in the NTF.

Stress analysis of the Pathfinder I wing determined a required minimum tensile yield strength (ref. 4) of 150 ksi and minimum plane-strain fracture toughness K_{Ic} (ref. 1) of 85 ksi-in$^{1/2}$ at -320°F. The plane-strain fracture toughness requirement was initially evaluated by correlation with Charpy impact strength by using the Barsom-Rolfe relationship (ref. 5):

$$K_{Ic} = \left[2E(CVN)^{3/2}\right]^{1/2}$$

where K_{Ic} is expressed in psi-in$^{1/2}$; Young's modulus E, in psi; and Charpy V-notch impact strength CVN, in ft-lb. However, this correlation was developed for ferritic steels and its validity for higher toughness materials was unknown. Charpy impact tests were conducted on specimens machined from a 5.5-in-thick plate obtained for model fabrication. The plate had been given a stress-relieving heat treatment, and yielded Charpy values which were considered too low to proceed with model development without conducting fracture toughness tests. (See ref. 6.)

Finite-element analysis (ref. 3) of the Pathfinder I wing determined that the location of peak stress occurred at the break in the wing planform (fig. 1). Aerodynamic measurements require placement of a row of pressure transducers at this location, but the effect this instrumentation would have on the fatigue behavior of the model wing during tunnel operation required evaluation.

This study was undertaken to explore the fracture resistance behavior of Nitronic 40 by using the single-edge-notch bend (SENB) specimen and to evaluate the fatigue response of a simple wing simulation specimen containing brazed plug orifices of a design considered for model fabrication.

This report presents the results of the fracture toughness and tensile property testing of Nitronic 40 at room and cryogenic temperatures and the results of fatigue testing of wing simulation specimens incorporating a brazing procedure for pressure transducer attachment.

SYMBOLS

A_1 area under load-deflection curve at maximum load, in-lb (fig. 14)

A_2 area under load-deflection curve at P_2, in-lb (fig. 14)

a effective crack length, in.

B specimen thickness, in.

CVN Charpy V-notch impact strength, ft-lb

c one-half specimen thickness, in.

E Young's modulus, psi

$f_1(a/w), f_2(a/w)$ polynomial expressions to account for specimen geometry effects on solution for K

I moment of inertia, in^4

J_{Ic} measure of toughness, ksi-in.

K stress intensity factor, $ksi\text{-}in^{1/2}$

K_{Ic} plane-strain fracture toughness, $ksi\text{-}in^{1/2}$

K_{Icd} equivalent energy fracture toughness, $ksi\text{-}in^{1/2}$

L plate longitudinal direction

L' plate orientation defined at 60° angle to plate longitudinal direction (fig. 2)

M specimen bending moment, in-lb

N number of cycles

P	applied specimen load, lb
P_2	load at arbitrary point along linear portion of load deflection curve, lb (fig. 14)
R	ratio of minimum to maximum load, P_{min}/P_{max}
S	load span, in.
T	plate transverse direction
T'	plate orientation defined at 60° angle to plate transverse direction (fig. 2)
v	crack mouth opening displacement, in.
W	specimen width, in.
δ	beam center deflection, in.
ε	strain, in/in.
$\dot{\varepsilon}$	strain rate, in/in/min
ν	Poisson's ratio
σ	applied stress, psi
σ_{tu}	ultimate tensile strength, psi
σ_{ty}	yield strength, psi

Subscripts:

max	maximum
min	minimum

Abbreviations:

LaRC	Langley Research Center
NTF	National Transonic Facility
RT	room temperature

MATERIALS, EQUIPMENT, AND PROCEDURES

Materials

All specimens utilized in this study were machined from a 5.5-in-thick, 44- by 60-in. Armco Nitronic 40 plate obtained for fabrication of the Pathfinder I wing. The composition of this plate is given in table I and compared with the nominal requirement. A stress-relieving heat treatment was performed on the plate at LaRC

according to the following schedule: 1350°F for 1 hr, 1800°F for 1 hr, 2000°F for 2 hr, and furnace cool to room temperature. The locations of specimens on the plate are shown in figure 2. Single-edge-notch bend (SENB) specimens (ref. 7) were machined from the plate prior to the stress-relieving heat treatment to measure the fracture resistance of material in the as-received condition. Additional SENB specimens were machined after the stress-relieving treatment. Specimen orientations were chosen to reflect toughness in the direction of wing loading (TS) and normal to this direction (TL). Specimen orientation designations are given relative to original plate directions.

Wing simulation specimens were machined at a 60° angle to the plate rolling direction, with the long axis parallel to the leading edge of the wing. Tensile specimens tested during this study were cut from a wing simulation specimen with axes along the length and width of the specimen. The resultant tensile properties are therefore measured at a 60° angle to the plate longitudinal and transverse directions.

Tensile Testing

Tensile specimens were machined from specimen blanks according to the dimensions shown in figure 3. The specimens were loaded in tension to determine yield and ultimate strengths and Young's modulus at both room temperature and -275°F. All testing was done with a closed-loop electrohydraulic, 55 000-lb capacity test machine. For cryogenic testing, an environmental chamber was attached to the test frame and cooled with liquid nitrogen to -275°F. Outputs from three strain gages, attached at 120° intervals around the specimen circumference (fig. 3), were monitored to determine axial strain during loading. Load was monitored through the test frame load cell. Room temperature specimens were loaded at an initial strain rate $\dot{\varepsilon}$ of 0.0007 in/in/min. Specimens tested at -275°F were loaded at $\dot{\varepsilon}$ = 0.0015 in/in/min initially.

A Hewlett-Packard 3052A data acquisition system, shown in figure 4, was used to record the test data. The system includes a desktop computer, digital and system voltmeters, a scanner, and a real-time clock. Specimen load, strain-gage output, and strain-gage bridge voltage were monitored and recorded. Tensile test monitoring and data collection were accomplished by using a computer program developed for static tensile testing. A computer program developed for data reduction was used to provide stress-strain curves and modulus determinations.

Fracture Toughness and Crack Growth Testing

Single-edge-notch bend specimens were machined to dimensions shown in figure 5 and tested at both room and cryogenic temperatures to obtain fatigue crack growth rates and fracture toughness estimates. All testing was conducted with a 100 000-lb-capacity closed-loop electrohydraulic test machine. For cryogenic testing, an environmental chamber was attached to the test frame and cooled with liquid nitrogen to -275°F (fig. 6). The chamber controller typically held the temperature to within 5°F of the desired test temperature. Specimens were fatigue precracked at both room and cryogenic temperatures to a crack length of approximately 0.50 in. by using a three-point bend apparatus shown in figure 7. Precracking was conducted at room temperature in order to obtain crack growth rates at ambient temperatures for comparison with the rates obtained in cryogenic tests.

A clip-on crack mouth opening displacement gage was attached to the integrally machined knife edges in the sample (fig. 7) to monitor crack mouth displacement. A compliance relationship was used to determine crack length during fatigue cycling. The compliance was taken as the ratio of crack mouth opening displacement v to specimen bending moment M. Due to specimen geometry and load span, the magnitude of the bending moment M in in-lb, is equal to the magnitude of the specimen load P, in lb. The relationship of crack length to compliance was determined by regression analysis of experimentally generated measurements of compliance and crack length for the notch bend specimen in cantilever bending (ref. 8). The compliance relationship gives effective crack length a as a function of specimen geometry, Young's modulus, and the ratio v/M:

$$a = W \exp\left\{-3.93 + 1.575\left[\ln\left(EBW\,\frac{v}{M}\right)\right] - 0.232\left[\ln\left(EBW\,\frac{v}{M}\right)\right]^2 + 0.0122\left[\ln\left(EBW\,\frac{v}{M}\right)\right]^3\right\}$$

Crack length is uniquely related to the compliance according to this regression equation. Thus, increases in crack length during fatigue cycling can be monitored through measurements of compliance.

Data collection was achieved by using the data acquisition system previously described, but data were obtained in these tests with a fatigue test computer program. The computer program recorded crack mouth opening displacement and load signals every 5000 cycles and calculated the compliance. Computer control was used to stop fatigue cycling by closing mechanical relays when the compliance had reached a preset maximum value corresponding to the desired crack length. The crack length determined by compliance at completion of precracking was generally within 3 percent of the fatigue crack length as measured visually after specimen fracture.

A regression analysis software package was used for basic data manipulation and analysis of crack growth data (ref. 9). Crack growth rate da/dN was obtained by curve-fitting plots of crack length versus number of cycles and by mathematically differentiating the regression equation. Stress intensity K levels were calculated based on specimen load and crack length for each interval of data collection. Plots of da/dN versus K were used to evaluate crack growth behavior.

Fracture toughness testing was accomplished by obtaining curves of load versus crack opening displacement for the precracked specimens in three-point bending. The curves were recorded autographically by a x-y recorder and then analyzed to determine fracture parameters.

Wing Simulation Testing

Rectangular specimens were machined to investigate the effects of instrumentation holes and brazed plugs on the fatigue behavior of the Pathfinder I wing. Six specimens of the type shown in figure 8 were machined through the thickness of the 5.5-in-thick plate at the location shown in figure 2. The hole drilled at a 60° angle across the specimen width represents a passageway for pressure transducer wiring. The four circular plugs represent the pressure transducers that are brazed into the upper wing surface at the peak stress location. The plugs were brazed into the specimens by using a proposed method for attaching pressure transducers to be considered as an alternative to the usual practice of soft soldering. The braze alloy

is 82 percent Au and 18 percent Ni applied according to the following schedule: 1350°F for 1 hr, 1650°F for 1 hr, 1825°F for 4 min, and furnace cool to room temperature.

The current model design criteria document (ref. 10) requires that a factor of safety of 3 based on yield be applied to the wing design, limiting the maximum wing stress to a very low value if a full stress concentration factor of 3 is applied to the brazed plug hole. All specimens were fatigue loaded in bending using the fixture shown in figure 9. Five specimens were loaded with a maximum bending moment corresponding to an outer fiber stress σ_{max} of approximately 1/3 the yield strength and a minimum bending moment of near zero outer fiber stress (R = 0.05). One of these specimens was tested at room temperature and four at -275°F. An additional test conducted at -275°F was used to simulate a buffeting load superimposed on a high static load, a condition which might be expected in tunnel operation. For this test the minimum bending moment during testing was adjusted to 75 percent of the maximum bending moment (R = 0.75).

Samples were cycled at a frequency of 10 cycles/sec for approximately 1 million cycles and evaluated for crack initiation. If crack initiation did not occur, the bending moment was increased by 10 percent. The million-cycle blocks of fatigue loading were continued stepwise, increasing σ_{max} until crack initiation occurred. The applied bending moment was then held constant and cycling continued until net section failure in order to obtain information on load-carrying behavior as fatigue crack growth continued.

Compliance was monitored during testing to detect changes in specimen stiffness caused by cracking. The ratio of deflection of the specimen center to the applied moment was taken as the compliance. Outer fiber stress was calculated from beam theory by using the value of applied bending moment and specimen geometry. A single strain gage was affixed to the center of four specimens on the tensile side of the beam to directly measure outer fiber strain. Outer fiber stress calculated from the strain-gage output was compared with that calculated from beam theory.

Four small crack propagation gages (ref. 11) were attached to each of the remaining two specimens, one over each brazed plug (fig. 10), to provide a precise account of crack initiation and growth. The crack propagation gage grid contains 20 elements over the 0.20-in. width. The gage behavior was monitored with appropriate signal conditioning such that initial output was adjusted to 10 mV and increased stepwise with each element failure to 100 mV when all elements had failed. Each gage element break and corresponding stepwise output voltage increase corresponds to a crack extension of 0.01 in.

The data acquisition system was used to monitor applied load, specimen deflection, and either strain-gage or crack propagation gage signals. Data collection was accomplished by using the fatigue control program as utilized in the crack growth tests but modified for the appropriate instrumentation utilized in each specific test. The regression analysis package (ref. 9) was used to provide basic data manipulation and analysis of compliance behavior, strain, or crack propagation behavior.

RESULTS AND DISCUSSION

Tensile Testing

Typical tensile stress-strain curves are shown in figure 11 for Nitronic 40 specimens tested at both room and cryogenic temperatures. The yield strength at -275°F is more than a factor of 2 greater than the room temperature yield strength. The greater slope of the elastic region of the curve generated at -275°F indicates a slight increase in Young's modulus at the low temperature as compared with that at room temperature. This difference is better represented in figure 12, which is a computer-generated plot of the secant modulus versus strain for each stress-strain curve. The initial horizontal portion of the curves represents the slope in the elastic region of each stress-strain curve and, thus, a measure of Young's modulus for the material. The modulus observed at the cryogenic test temperature is about 4 percent higher than that at room temperature based on average values.

The tensile properties of Nitronic 40 supplied by the manufacturer, Armco Steel Corporation, and from preliminary property testing conducted at LaRC, along with properties determined in the current study are presented in table II. The data supplied by Armco reflects properties of annealed plate. The preliminary tests at LaRC were conducted with 0.2- by 0.25-in. rectangular tensile specimens machined from the 5.5-in-thick plate after the stress-relieving heat treatment. The current data, generated by testing 0.5-in-diameter round tensile specimens cut from the wing simulation specimen, represent 60° off-axis properties of stress-relieved plate which has also undergone the brazing cycle described in the procedure in the section "Wing Simulation Testing."

Data from all testing are represented graphically in figure 13. The stress-relieving and brazing cycles result in lowered tensile mechanical properties. At room temperature, decreases in yield strength of approximately 13 percent and 17 percent were observed for material in the stress-relieved and stress-relieved and brazed conditions, respectively, as compared with the trend of data for annealed plate. At -275°F, the decreases observed in yield strength were approximately 10 percent and 12 percent as compared with the trend for annealed plate. No significant variation in strength was observed relative to specimen orientation (table II). The Nitronic 40 plate supplied to LaRC was reported to be cross-rolled during processing (ref. 6), which would account for the relatively isotropic properties observed.

The percent reduction in tensile yield strength observed due to the stress-relieving and brazing cycles appeared consistent at room temperature and -275°F. Although testing was not conducted below -275°F for material in the stress-relieved and brazed condition, a similar percent reduction might be expected. Thus, the tensile yield strength observed at -320°F for material in the stress-relieved and brazed condition would be in the 140 000-psi range.

Fracture Toughness Testing

Fracture toughness tests were conducted with single-edge-notch bend specimens and the test procedure outlined in the ASTM standard for plane-strain fracture toughness K_{Ic} testing (ref. 7). Estimates of toughness from Charpy testing indicated that Nitronic 40 retains such ductility at cryogenic temperatures that it would be impractical if not impossible to test a specimen large enough to obtain a valid K_{Ic} value. For this reason, specimen size was selected to be representative of the actual model size, and the test results were then analyzed according to the equiva-

lent energy method developed by Witt (ref. 12) in order to obtain an estimate of the toughness from data collected.

A typical load-deflection curve for the fracture toughness test is shown in figure 14, with the parameters for Witt's method indicated. The equivalent energy fracture toughness K_{Icd} is given by the following equation for the single-edge-notch bend specimen (ref. 13):

$$K_{Icd} = \frac{P_2 S(A_1/A_2)}{BW^{3/2}} f_1(a/w)$$

where

$$f_1(a/W) = 2.9(a/W)^{1/2} - 4.6(a/W)^{3/2} + 21.8(a/W)^{5/2}$$

$$- 37.6(a/W)^{7/2} + 38.7(a/W)^{9/2}$$

In reference 13, this relation has shown that K_{Icd} is a good estimate for K_{Ic} for materials with fracture toughness values greater than 200 ksi-in$^{1/2}$.

The values of K_{Icd} for all test conditions, tabulated by heat treatment, orientation, and precrack temperature, are presented in table III. The toughness of Nitronic 40 as estimated by the equivalent energy method is extremely high (approximately 350 ksi-in$^{1/2}$); this indicates that failure of the material would occur by gross yielding of the net section and not by unstable crack growth based on Pathfinder I dimensions. All notch bend specimens tested failed by plastic hinge of the remaining ligament.

The values of K_{Icd} determined are slightly greater for all cases in the stress-relieved condition than in the as-received condition. There is no significant difference in toughness due to specimen orientation; again, this suggests isotropic properties. As might be expected, the temperature at which specimens were fatigue precracked did not affect toughness at -275°F.

Tobler and Reed (ref. 14) have evaluated the toughness of 21-6-9 (previous designation for Nitronic 40) in the annealed condition by using the J-integral technique. An estimate of the plane-strain fracture toughness K_{Ic} was made from the value of J_{Ic} obtained by the following equation from reference 15:

$$K_{Ic}^2 = \frac{EJ_{Ic}}{1 - \nu^2}$$

Measurements of J_{Ic} were obtained at -320°F and resulted in an estimate of K_{Ic} of 250 ksi-in$^{1/2}$. The estimates of K_{Ic} obtained during the current testing are in reasonable agreement with the results of Tobler and Reed, and the differences may be related to temperature, orientation, or metallurgical condition.

Fatigue Crack Growth Testing

Fatigue crack growth behavior was examined over a small region of stress intensity factor range ΔK by monitoring the crack growth observed during precracking prior to the fracture toughness test. A representative plot of crack length versus number of cycles is shown in figure 15. Regression analysis was used to calculate the crack growth rate da/dN by using the method discussed in the section "Fracture Toughness and Crack Growth Testing." Since a log-log plot of da/dN versus ΔK is often a straight line, the rate of crack growth during fatigue can be related to the stress intensity factor range ΔK by the power function (ref. 16):

$$\frac{da}{dN} = c(\Delta K)^n$$

where c and n are material constants. The stress intensity factor range is calculated from the expression (ref. 7):

$$\Delta K = \frac{\Delta P}{BW^{3/2}} f_2(a/W)$$

where ΔP is the range of specimen load in pounds, and

$$f_2(a/W) = \frac{3(a/W)^{1/2}\{1.99 - (a/W)(1 - a/W)[2.15 - 3.93a/W + 2.7(a/w)^2]\}}{2(1 + 2a/W)(1 - a/W)^{3/2}}$$

Figure 16 is a composite plot of da/dN versus ΔK on log-log scales for all test data. At ΔK values less than about 25 ksi-in$^{1/2}$, crack growth occurs more rapidly at -275°F than at room temperature. Above a value of ΔK of 25 ksi-in$^{1/2}$, the crack growth rates are comparable for both temperatures. Figures 17 and 18 illustrate the effects of heat treatment and specimen orientation on crack growth rates. Figure 17 is a plot of two TS (fig. 2) specimens tested at -275°F; one is in the as-received (annealed) condition and the other was stress relieved. No significant difference in crack growth behavior was noted for these cases. Figure 18 shows the crack growth curves of two specimens tested at room temperature and differing only in specimen orientation. There is no significant effect of orientation in the overlapping region of ΔK.

Wing Simulation Testing

Specimen compliance curves for the room temperature test, a cryogenic test with near zero minimum stress, and the cryogenic test with loading to simulate buffeting are shown in figures 19(a), (b), and (c), respectively. The loading history for each test, expressed as maximum outer fiber stress, is also shown in each figure. The maximum outer fiber stress σ_{max} is calculated from the maximum specimen load by using the relationship from beam theory: $\sigma = Mc/I$. Calculation of moment of inertia was done for this specimen configuration to account for the oblique hole across the

specimen width. For this specimen configuration and load span, specimen bending moment is numerically equal to twice the specimen load, M = 2P. Output from a single strain gage on the specimen surface was periodically recorded and used to calculate specimen outer fiber stress. These stress values are plotted in figure 19(a) on the load history curve as solid triangular symbols and are in close agreement with values calculated by using the beam theory relationship (open square symbols). Material yield strength σ_{ty} at test temperature is indicated for each test.

Crack initiation was visually detected on the surface of the specimen tested at room temperature (fig. 19(a)) after about 7 million fatigue cycles and a stepwise increase in maximum outer fiber stress of six steps from 30 percent to 60 percent of the yield strength at room temperature. Significant crack growth is indicated by a sudden increase in compliance value. As can be seen in figure 19(a), there was no significant detectable change in compliance upon crack initiation. (A change in compliance was not observed until about 7.5 million cycles.) This lack of detection is related to difficulties in measuring the small changes in specimen deflection during fatigue loading. Fatigue loading was interrupted at crack initiation to observe any permanent deflection in the specimen prior to failure. After 7 million cycles of loading, a permanent deflection of 0.030 in. was observed from specimen end to centerline. Cycling was again interrupted after an additional 300 000 cycles and crack length was measured. In this specimen, cracks initiated at the brazed plug-base metal interface of plug I and plug III (fig. 8). Fatigue cracks extended across the specimen width from the plugs as shown in figures 20 and 21, and total crack lengths were measured to be 0.472 in. at plug I and 1.078 in. at plug III. Fatigue cycling was resumed and the maximum outer fiber stress was increased by 10 percent to 38 600 psi (nearly 80 percent of σ_{ty}). The rapid increase in compliance shown at about 7.8 million cycles in figure 19(a) is associated with the rapid crack growth which occurred when fatigue cycling at the increased stress level was begun. Cycling was stopped after 112 000 additional cycles. Crack lengths were measured to be 0.75 in. at plug I and 1.625 in. at plug III. Specimen deflection was increased to 0.412 in. but the specimen could still sustain the maximum applied bending moment. Permanent deflection prior to failure could be an important factor in determining wing cracking during an actual wind-tunnel test or in affecting aerodynamic factors (such as drag and angle of attack) during tunnel operation.

The compliance and load history curves shown in figure 19(b) are representative of those specimens tested at -275°F with high stress ranges (R = 0.05). In each of these tests, cracking initiated at maximum outer fiber stress levels between 40 percent and 45 percent of the yield strength at -275°F. For the specimen shown in figure 19(b), crack initiation as indicated by change in compliance was determined to occur at about 1.4 million cycles and a stress level of 45 percent of the yield strength. Visual examination for crack initiation was not performed in these cryogenic tests. Crack propagation gages were used on this specimen and indicated crack initiation occurred at 1.21 million cycles. Crack propagation occurred rapidly in all these tests. For the specimen shown in figure 19(b), failure by net section overload occurred after an additional 350 000 cycles.

The starting σ_{max} for each of these tests at -275°F and for the room temperature test was chosen equal to one-third the material yield strength in order to evaluate the stress concentration effect of the brazed plugs. In these tests, crack initiation occurred only after outer fiber stress was increased to 60 percent of the yield stress at room temperature and 40 to 45 percent at -275°F; this indicated that the brazed plugs did not affect the stress level in the manner of a finite hole.

Actual wind-tunnel models would not experience a loading history as severe as that imposed in the preceding tests. The model will likely experience a small cyclic load due to buffeting superimposed on a high static load. Compliance and load history curves for the specimen tested to simulate this buffeting condition are shown in figure 19(c). This test was conducted at -275°F and the specimen was subjected to a range of bending moment such that the minimum outer fiber stress was equal to 75 percent of the maximum outer fiber stress (R = 0.75). The starting maximum stress was chosen to be 50 percent of the yield strength. Four crack propagation gages were affixed to this specimen, one centered over each brazed plug. Visual examination for crack initiation was performed at intervals of about 1 million cycles. Examination after 2 million fatigue cycles revealed no specimen cracking. However, after 3 million cycles and an increase in maximum outer fiber stress to 60 percent of the yield strength, a crack approximately 0.68 in. in total length (fig. 22) was observed extending in both directions from plug II (fig. 8). There was no measurable permanent specimen deflection at this time. The data in figure 19(c) indicate no measurable change in specimen compliance until approximately 3.3 million cycles. At approximately 3.7 million cycles the compliance began rapidly increasing with each reading (readings are taken at 5000-cycle increments); this increase indicates a change in stiffness due to crack growth and gross yielding. Loading was terminated after about 3.8 million cycles and a permanent deflection of 0.18 in. was measured. The crack length was measured to be approximately 1.7 in. long.

Visual examination of both the specimen tested at room temperature and the specimen tested to simulate the buffeting condition indicate that the specimen stiffness and, hence, the compliance measurement is insensitive to cracking until a relatively large crack exists. Crack propagation gages were used to indicate crack initiation in two cryogenic tests. This crack initiation and early growth are represented by a plot of crack propagation gage output versus cycles as shown in figure 23. The output from one gage on each specimen at the plug where crack initiation and growth occurred is presented for comparison. The load-cycle history for one of the specimens is associated with the specimen represented in figure 19(b) (R = 0.05), and the other with the specimen represented in figure 19(c) (R = 0.75). During the test at R = 0.05, crack initiation occurs at about 1.2 million cycles. The gage represented is completely failed at 1.35 million cycles. The gage output represents crack growth of 0.20 in. in approximately 150 000 cycles. Visual examination of the specimen tested at R = 0.75 at 2 million cycles revealed no specimen cracking but did reveal damage to the crack propagation gage on plug II, as shown in figure 24. The braze joint for this plug was not complete, causing several elements of the gage to break on the first load cycle. Visual examination at 3 million cycles did reveal a fatigue crack; therefore, the voltage step shown for this gage at just above 2 million cycles (fig. 23) represents the first gage element break due to fatigue and thus crack initiation of the specimen tested at R = 0.75. Crack propagation across this gage is complete at 3.07 million cycles, representing crack growth of 0.03 inch in nearly 1 million cycles.

The data exemplify the importance of stress range on crack growth. Even though the magnitude of the maximum stress was much greater during the test at R = 0.75, the time to crack initiation was significantly longer and crack growth was much slower compared with the test at R = 0.05. This difference is related to the lower stress excursion per cycle in the test at R = 0.75. Crack propagation gages were useful in providing accurate indications of crack initiation and early crack growth. Crack propagation gages could be useful in establishing braze joint integrity when used in conjunction with proof loading and could be useful in assessing structural degradation in actual hardware. The compliance measurement recorded is a useful

method of providing an indication of later stages of crack growth but is not sensitive to very early crack growth. Combining these methods of measurement will provide a reliable means of indicating specimen fatigue crack behavior.

The load history and performance of the specimen tested at $R = 0.75$ indicated that much fatigue damage could be endured and would likely be identified before major structural degradation or failure would occur if loads were not substantially increased by aerodynamic changes or tunnel operational parameters. The test at $R = 0.75$ and -275°F simulates likely wind-tunnel operating conditions. Specimen crack initiation during this test did not occur until a stress level of 60 percent of the yield strength was reached, and then crack growth was observed to proceed very slowly.

In every test case, cracks initiated at the brazed plug-base metal interface. Separation of the plug from the base metal through the braze joint typically occurred for about 180° around the plug before cracking in the base metal began. None of the plugs were completely expelled from the specimen nor did they appear to move relative to the surface to which they remained brazed. The plugs remained circular and intact with crack propagation progressing into the base metal. These results indicate the braze attachment technique to be an effective means of affixing the pressure-transducer instrumentation system and suggest that the system should be able to withstand conditions expected in wind-tunnel testing without degradation.

CONCLUSIONS

A test program was conducted to evaluate the fracture resistance and fatigue response of Armco Nitronic 40 austenitic stainless steel under cryogenic test conditions. Tensile, fatigue crack growth, and fracture toughness property measurements were made at -275°F. A study was conducted to evaluate the behavior of a simulated wing-section and pressure-transducer attachment under simulated NTF loading and temperatures. Analysis of the results of these experiments led to the following conclusions regarding both material capabilities of Nitronic 40 for application in cryogenic-wind-tunnel models and test methodology employed in assessing material behavior exposed to the NTF operating conditions.

1. Nitronic 40 displays a combination of strength and toughness at -275°F which may be adequate for application as a wind-tunnel model material at this temperature. An estimate of fracture toughness (K_{Ic}) by the equivalent energy technique of 350 ksi-$in^{1/2}$ at -275°F greatly exceeds the value determined by the Barsom-Rolfe equation for the impact strength measured for this material.

2. Measurements of Nitronic 40 toughness by using the equivalent energy technique indicate a fracture toughness value so high that failure would occur by gross yielding rather than unstable crack growth. Fatigue crack initiation and growth would be more critical to structural integrity than fracture toughness.

3. Wing simulation specimen test results suggest that Nitronic 40 could be used at stress levels approaching 60 percent of the yield strength at room temperature (for $R = 0.05$) and at -275°F (for $R = 0.75$). (The symbol R is the ratio of minimum to maximum load.)

4. A brazing technique for pressure-transducer attachment is an effective method for transducer plug insertion when both high stress levels and large temperature excursions may be experienced.

5. Compliance measurement techniques are valid methods for indication of crack growth in fatigue test specimens but are not sensitive indications of crack initiation.

6. Crack propagation gages were highly effective in providing for accurate determination of crack initiation and early crack growth in test specimens.

Langley Research Center
National Aeronautics and Space Administration
Hampton, VA 23665
April 17, 1984

REFERENCES

1. Hudson, C. Michael: Material Selection for the Pathfinder I Model. Cryogenic Technology, NASA CP-2122, Part II, 1980, pp. 423-441.

2. Armco NITRONIC 40 Stainless Steel Bar and Wire. S-54, Armco Steel Corp.

3. Howell, Robert R.: Overview of Engineering Design and Operating Capabilities of the National Transonic Facility. Cryogenic Technology, NASA CP-2122, Pt. I, 1980, pp. 49-75.

4. Hunter, William F.: Analysis and Testing of Model/Sting Systems. Cryogenic Technology, NASA CP-2122, Part II, 1980, pp. 411-422.

5. Barsom, J. M.; and Rolfe, S. T.: Correlations Between K_{IC} and Charpy V-Notch Test Results in the Transition-Temperature Range. Impact Testing of Metals, ASTM STP 466, 1970, pp. 281-302.

6. Wigley, D. A.: The Metallurgical Structure and Mechanical Properties at Low Temperature of Nitronic 40, With Particular Reference to Its Use in the Construction of Models for Cryogenic Wind Tunnels. NASA CR-165907, 1982.

7. Standard Test Method for Plane-Strain Fracture Toughness of Metallic Materials. ASTM Designation: E 399 - 81. Part 10 of 1982 Annual Book of ASTM Standards, 1982, pp. 592-622.

8. Lisagor, W. Barry: Influence of Precracked Specimen Configuration and Starting Stress Intensity on the Stress Corrosion Cracking of 4340 Steel. Paper presented at ASTM-NBS Symposium on Environment Sensitive Fracture: Evaluation and Comparison of Test Methods (Gaithersburg, Maryland), Apr. 26-28, 1982.

9. Regression Analysis - Part No. 09845-15011. Hewlett Packard.

10. Wind-Tunnel Model Systems Criteria. LHB 8850.1, NASA Langley Res. Cent., Sept. 1981, ch. III.

11. Crack Propagation Gages. PB-110-3, Micro-Measurements Div., Vishay, c.1976.

12. Witt, F. Joel: The Equivalent Energy Method: An Engineering Approach to Fracture. Eng. Fract. Mech., vol. 14, no. 1, 1981, pp. 171-187.

13. Witzke, W. R.; and Stephens, J. R.: Comparison of Equivalent Energy and Energy Per Unit Area (W/A) Data With Valid Fracture Toughness Data for Iron, Aluminum, and Titanium Alloys. J. Test. & Eval., vol. 6, no. 1, Jan. 1978, pp. 75-79.

14. Tobler, R. L.; and Reed, R. P.: Tensile and Fracture Behavior of a Nitrogen-Strengthened, Chromium-Nickel-Manganese Stainless Steel at Cryogenic Temperatures. Elastic-Plastic Fracture, J. D. Landes, J. A. Begley, and G. A. Clarke, eds., ASTM STP 668, 1979, pp. 537-552.

15. Landes, J. D.; and Begley, J. A.: Test Results from J-Integral Studies: An Attempt To Establish a J_{Ic} Testing Procedure. Fracture Analysis, ASTM STP 560, 1974, pp. 170-186.

16. Broek, David: Elementary Engineering Fracture Mechanics. Sijthoff & Noordhoff, c.1974, p. 230.

TABLE I.- COMPOSITION OF NITRONIC 40 STAINLESS STEEL PLATE

Element	Nominal composition, percent by weight	Actual plate composition, percent by weight
Carbon	0.08 max	0.026
Manganese	8.00 to 1.00	9.30
Phosphorus	.06 max	.021
Sulphur	.03 max	.003
Silicon	1.00 max	.67
Chromium	19.00 to 21.50	20.32
Nickel	5.50 to 7.50	6.68
Nitrogen	.15 to .40	.29
Aluminum	Balance	Balance

TABLE II.- TENSILE PROPERTIES OF NITRONIC 40 AUSTENITIC STAINLESS STEEL PLATE

Temperature, °F	Annealed[a]			Stress relieved[b]			Stress relieved[c] and brazed		
	Orientation	σ_{tu}, ksi	σ_{ty}, ksi	Orientation	σ_{tu}, ksi	σ_{ty}, ksi	Orientation	σ_{tu}, ksi	σ_{ty}, ksi
75	T	103.0	58.0	L'	101.0	50.3	L' T'	103.5 101.0	47.3 49.5
-110	T	134.0	87.0						
-275				L'	185.5	123.0	L' T'	158.5 158.5	119.4 119.0
-320	T	203.0	150.0						
-423	T	245.0	196.0						

[a]Data from reference 2.
[b]Data from preliminary tests at LaRC.
[c]Data from current study, average of two specimens.

TABLE III.- K_{Icd} FRACTURE TOUGHNESS VALUES (ksi$\sqrt{in}$) OF NITRONIC 40 AT -275°F

Precrack temperature, °F	Annealed		Stress relieved	
	Orientation	K_{Icd}, ksi-in$^{1/2}$	Orientation	K_{Icd}, ksi-in$^{1/2}$
75	TS	[b]281.6	TS	[a]389.3
	TL		TL	[c]393.9
-275	TS	[d]336.0	TS	[c]369.0
	TL	[c]301.0	TL	[b]394.0

[a]Average of three tests.
[b]Average of two tests.
[c]Result from single test.
[d]Average of six tests.

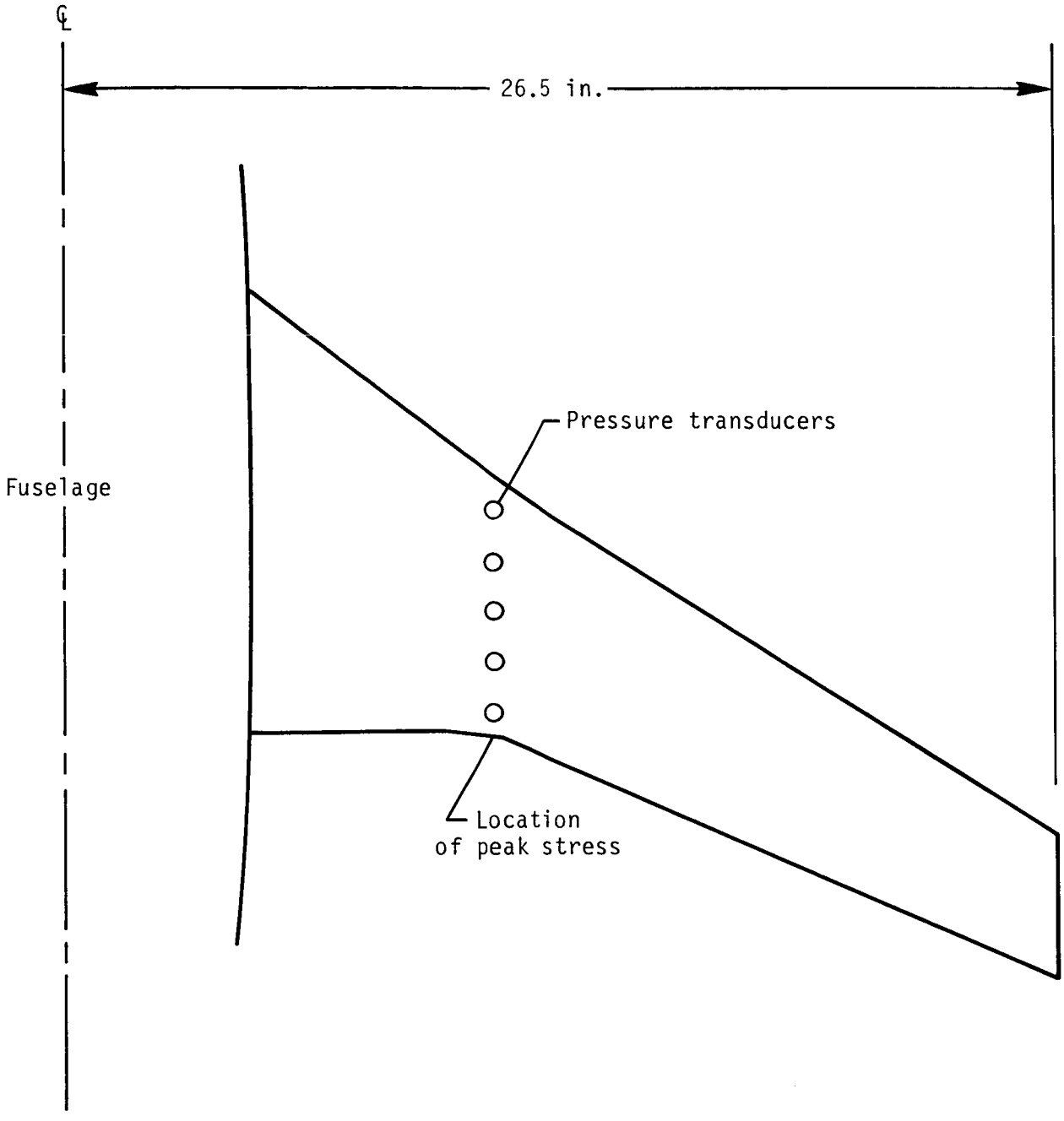

Figure 1.- Pathfinder I wing planform.

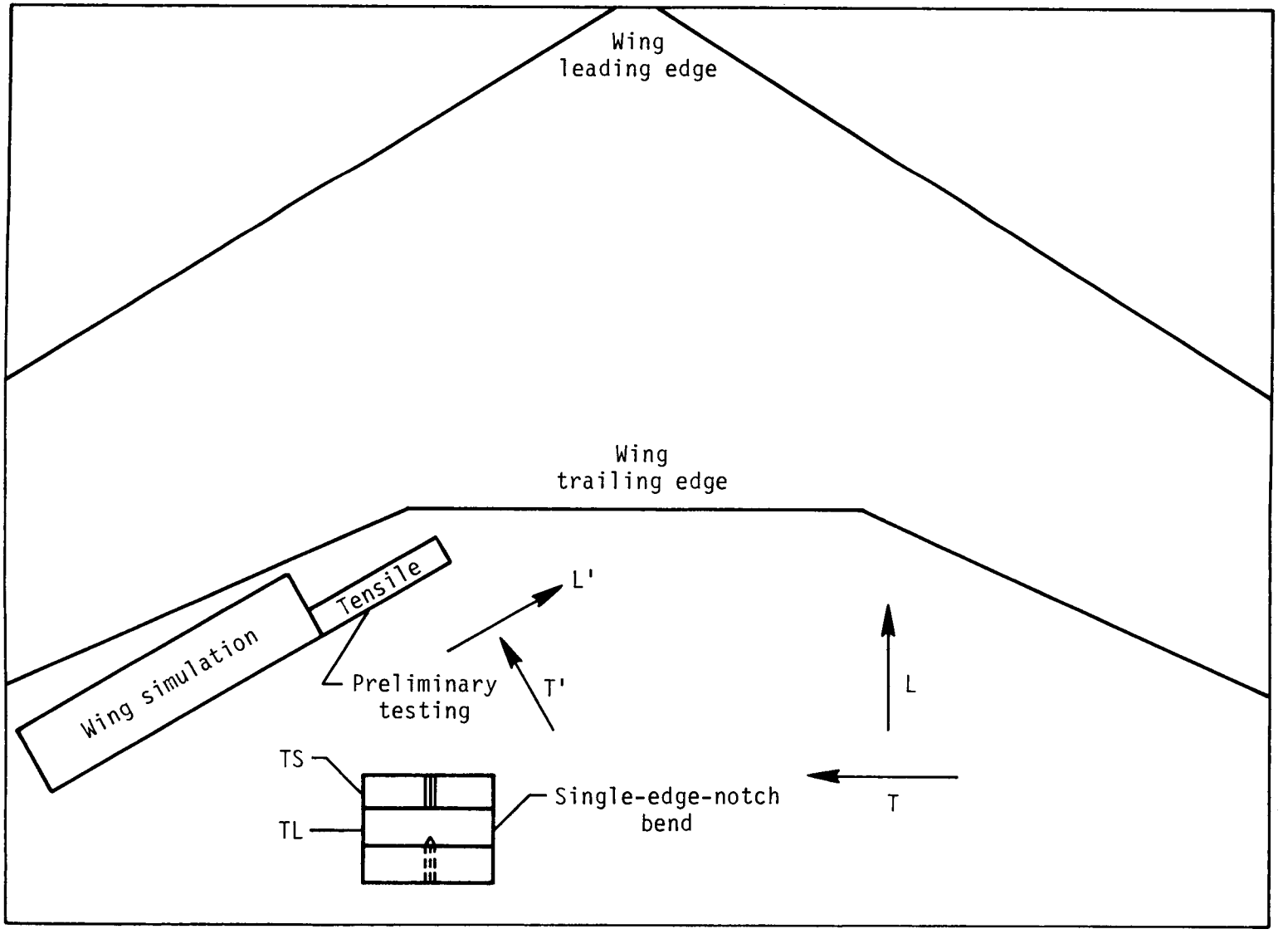

Figure 2.- Specimen locations on Nitronic 40 plate.

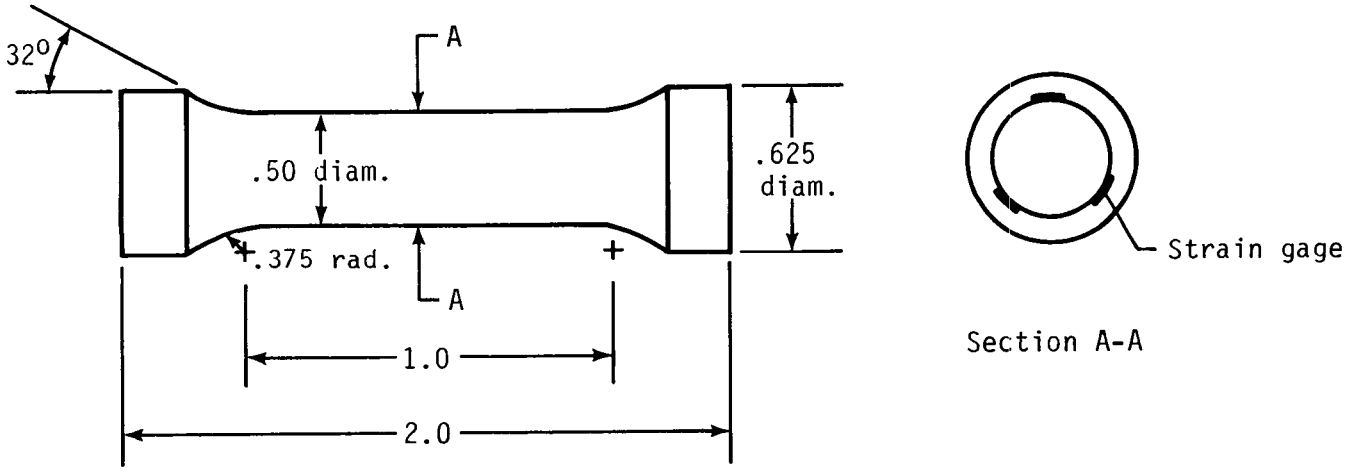

Figure 3.- Tensile specimen configuration. Dimensions are in inches.

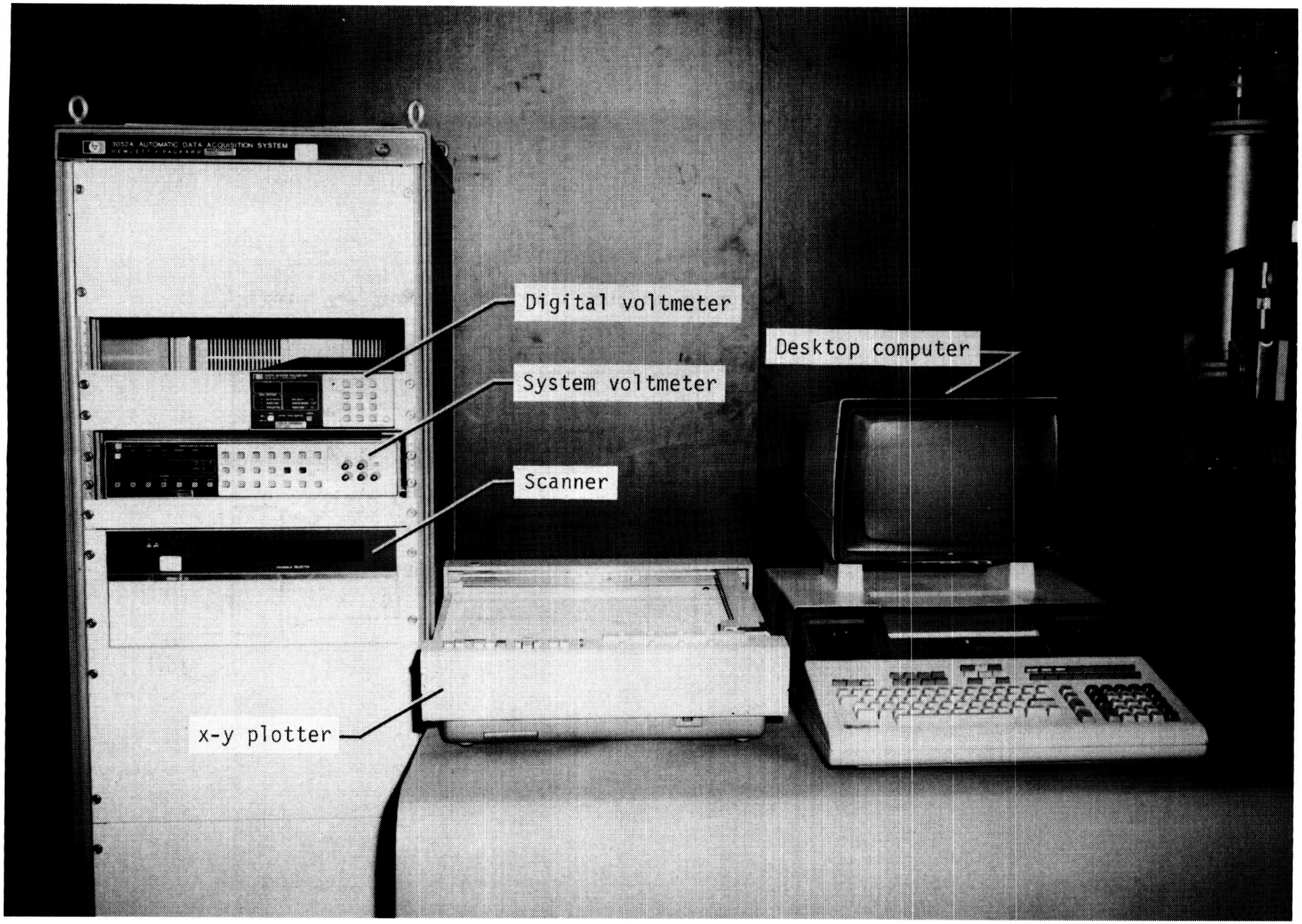

L-83-543.1

Figure 4.- Data acquisition system.

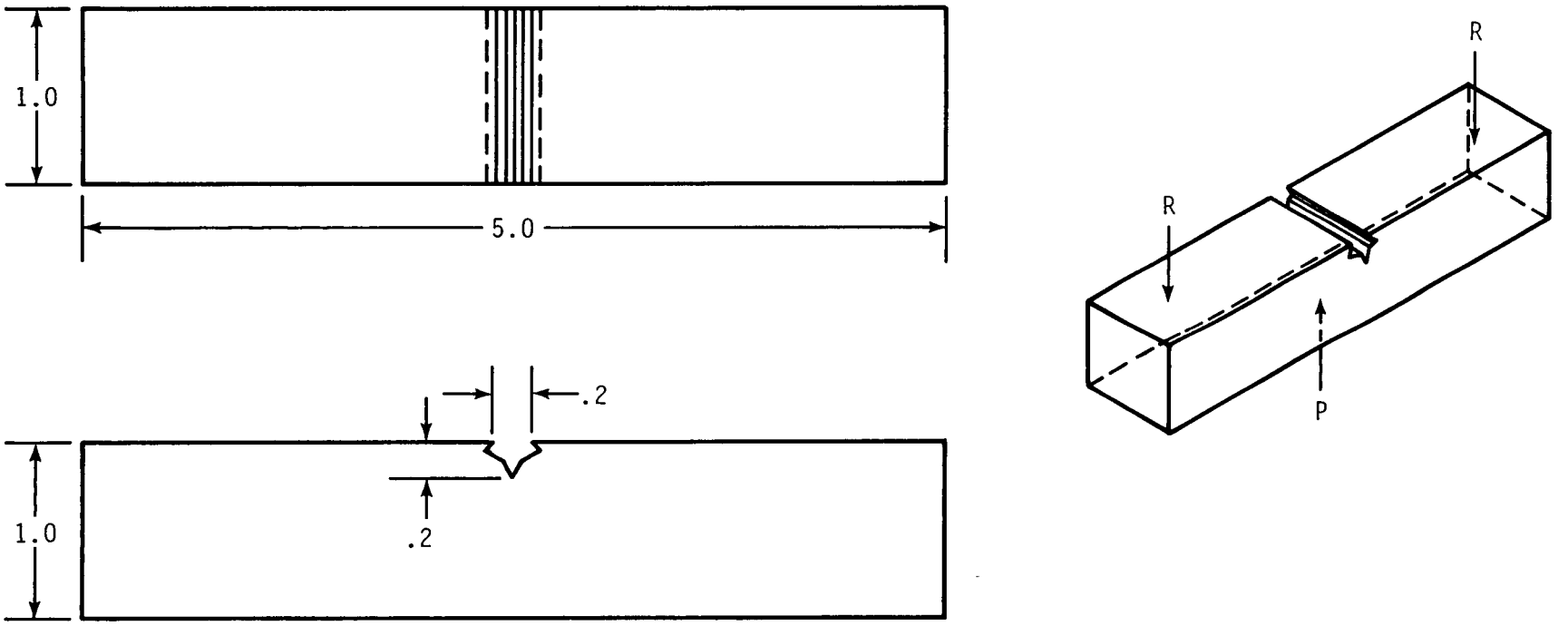

Figure 5.- Single-edge-notch bend specimen. Dimensions are in inches.

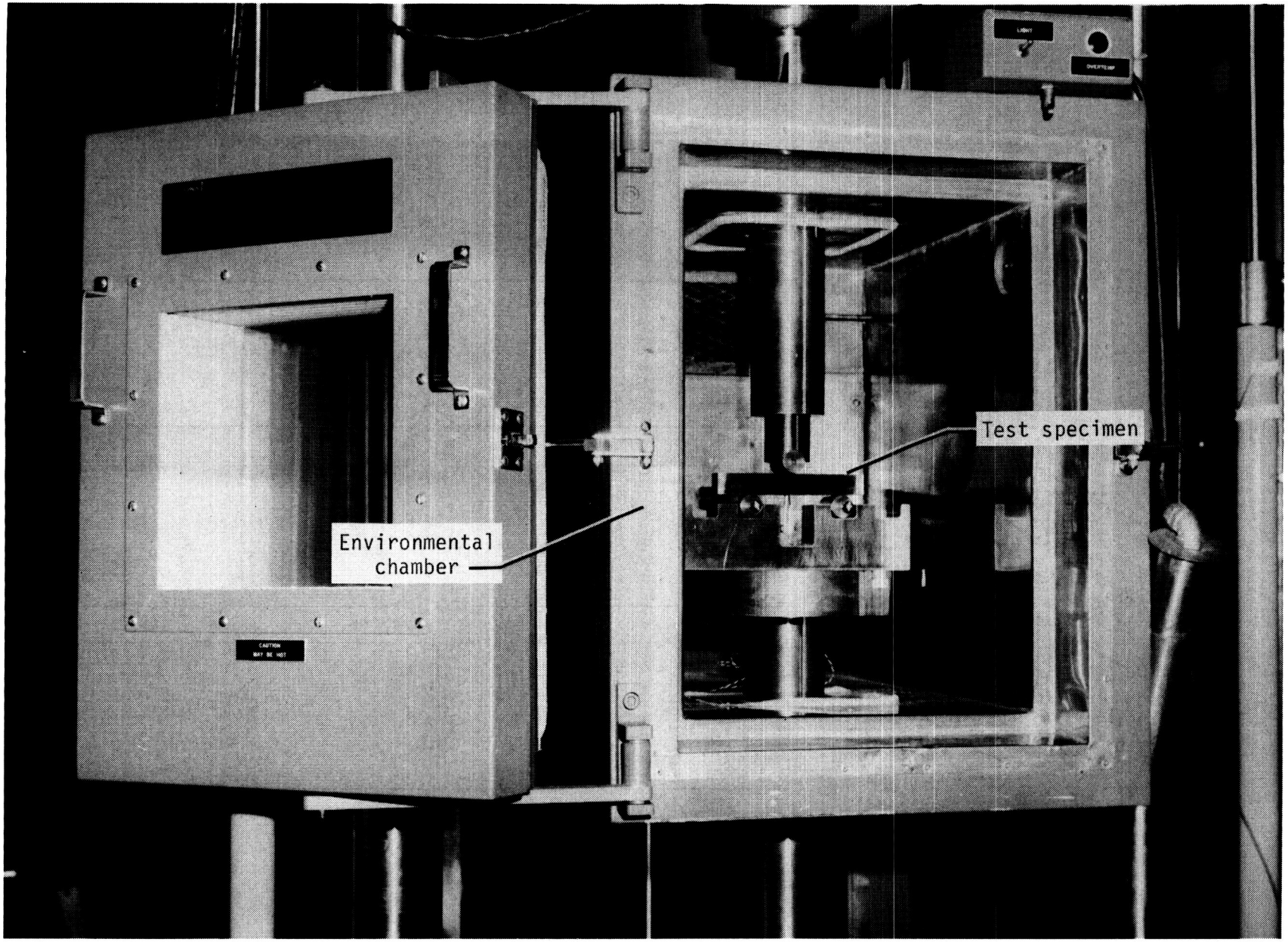

L-83-5155.1

Figure 6.- Environmental chamber used to achieve cryogenic environment.

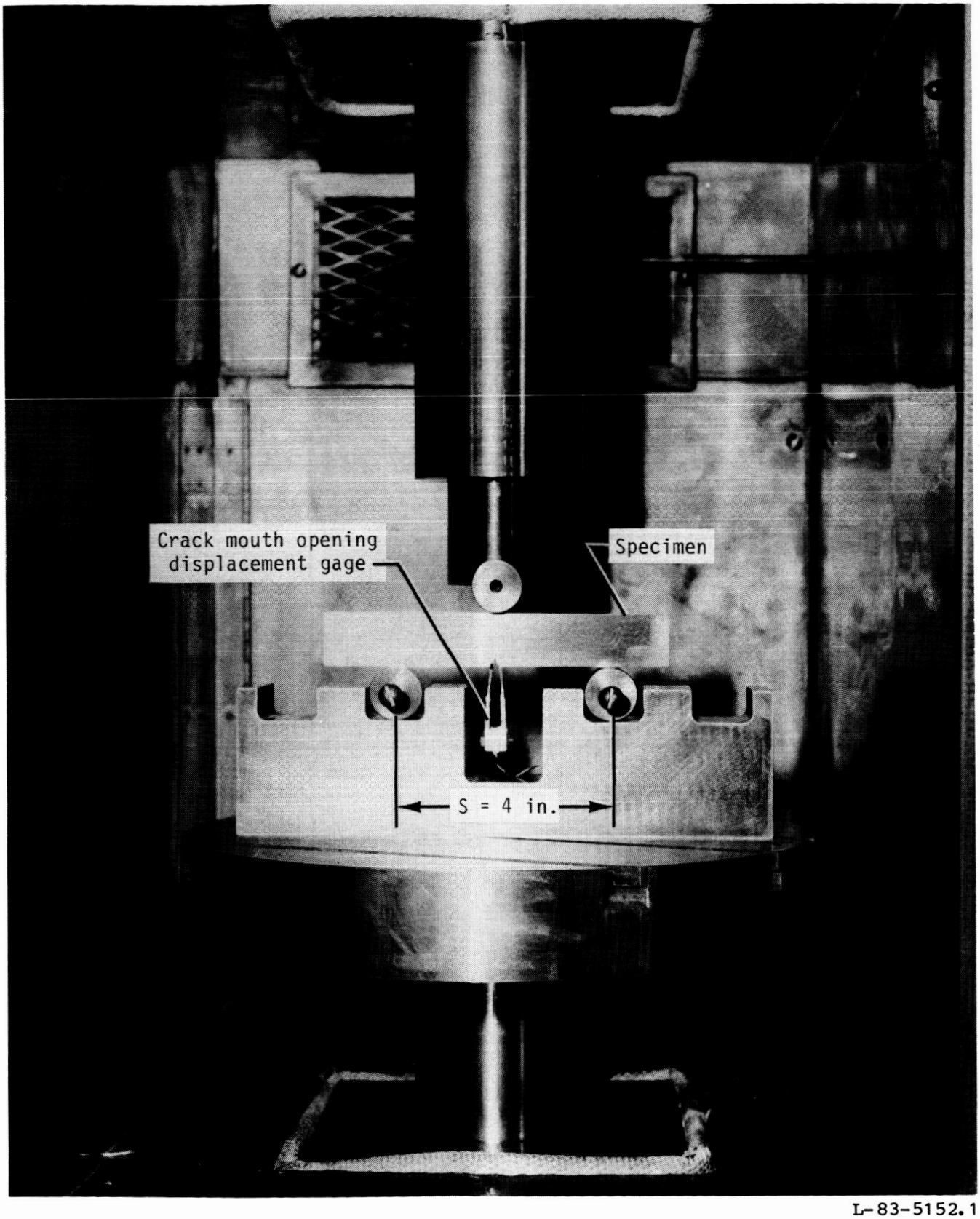

L-83-5152.1

Figure 7.- Three-point bend apparatus for fatigue crack growth and fracture toughness testing.

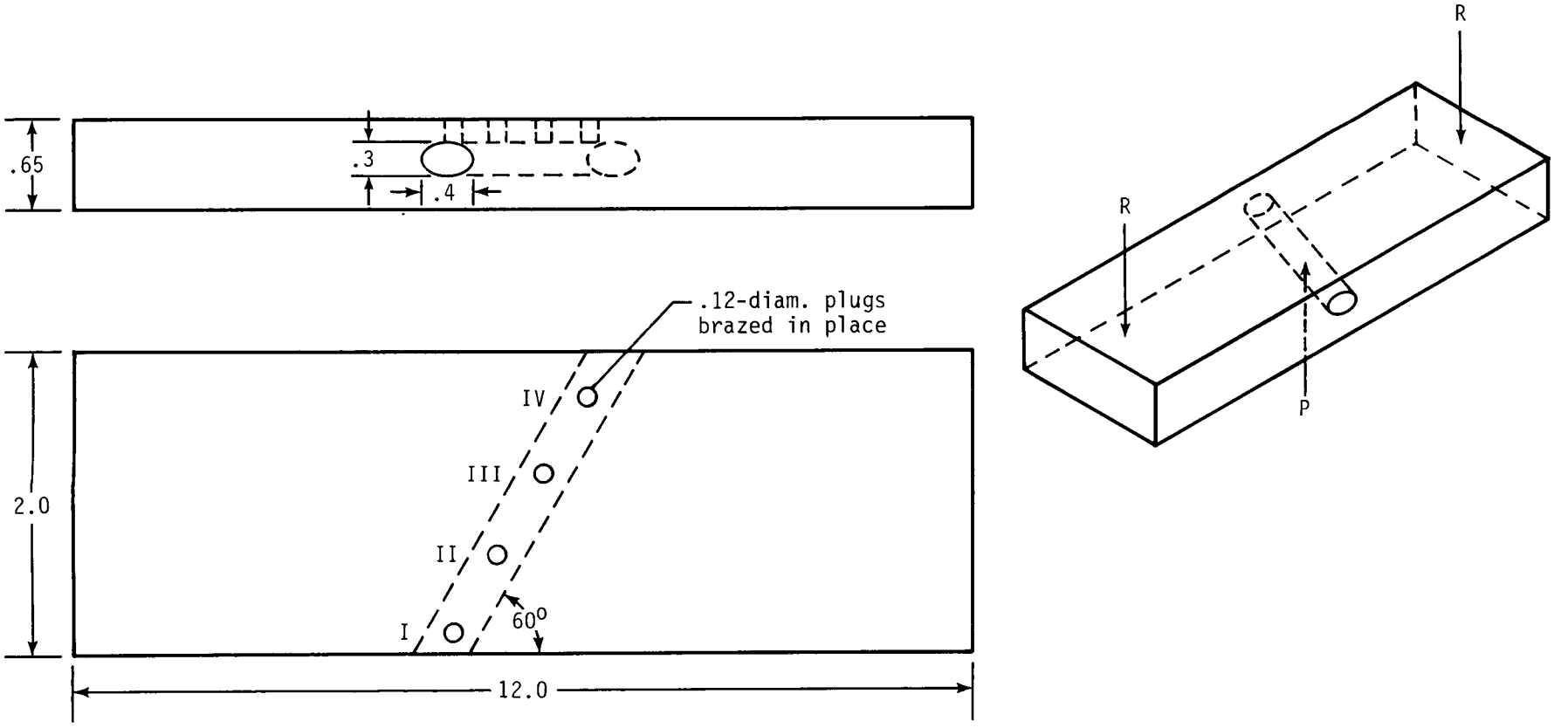

Figure 8.- Wing simulation specimen. Dimensions are in inches.

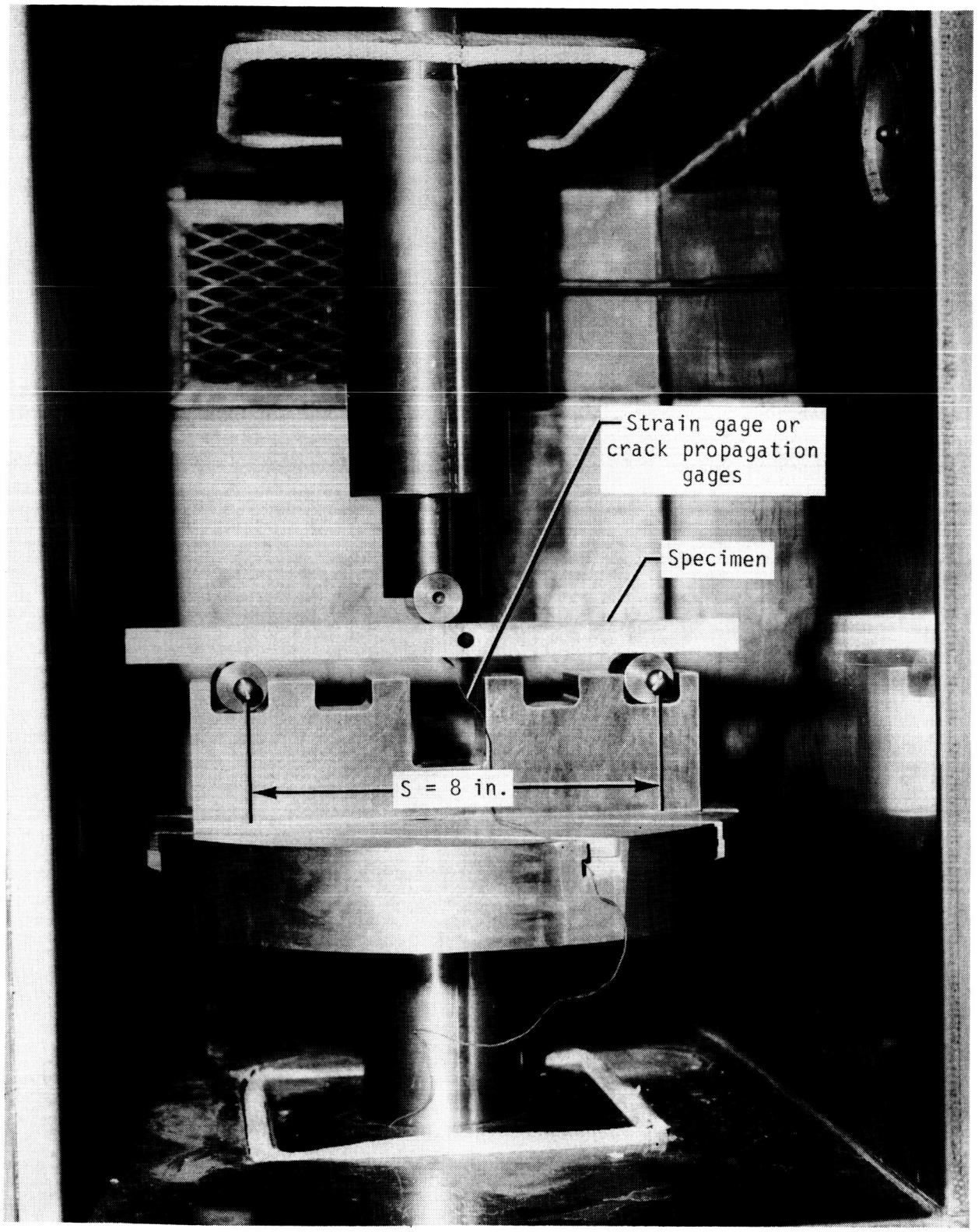

L-83-5153.1

Figure 9.- Three-point bend apparatus for fatigue loading wing simulation specimens.

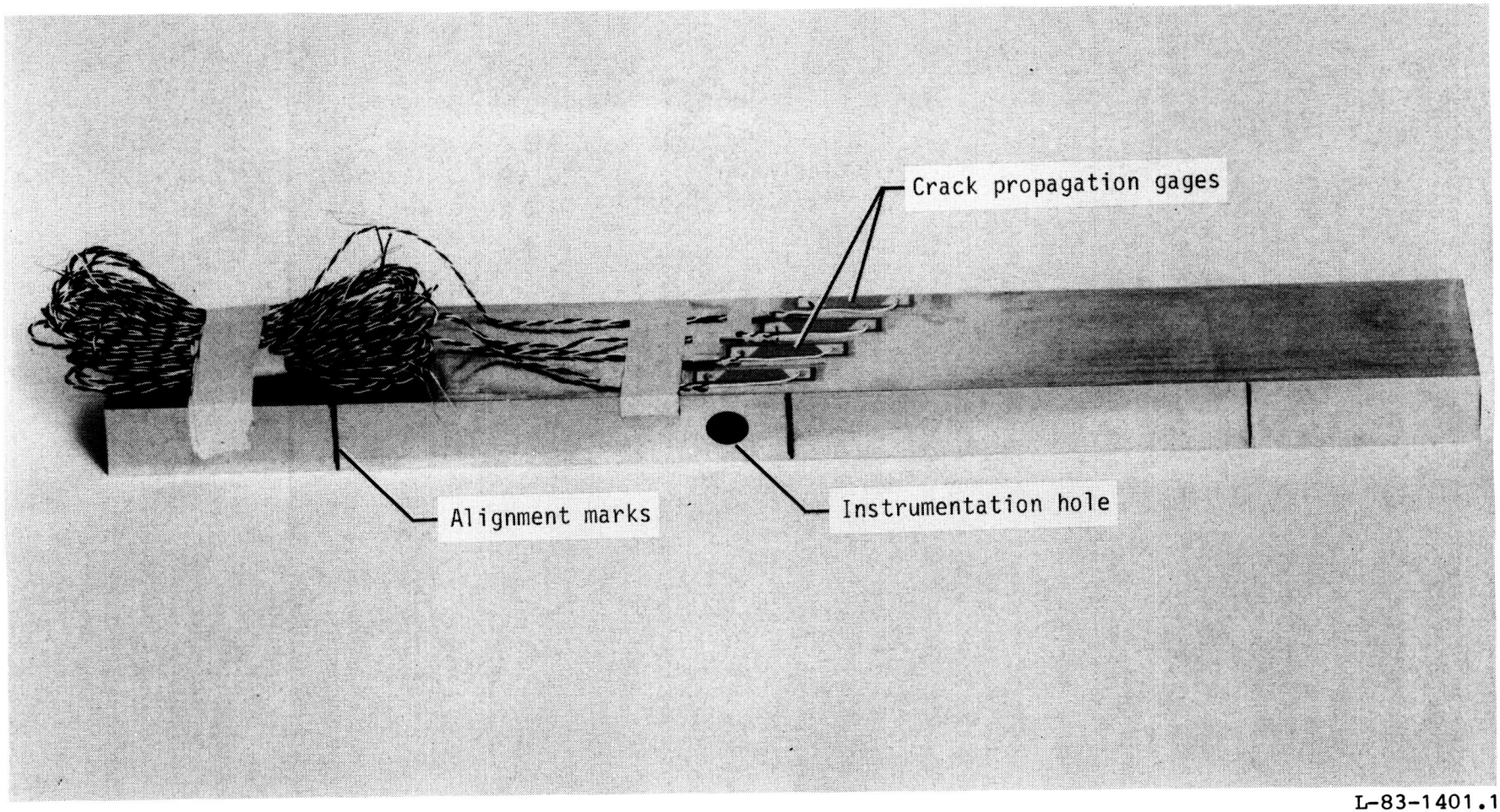

L-83-1401.1

Figure 10.- Crack propagation gage attachment on wing simulation specimens.

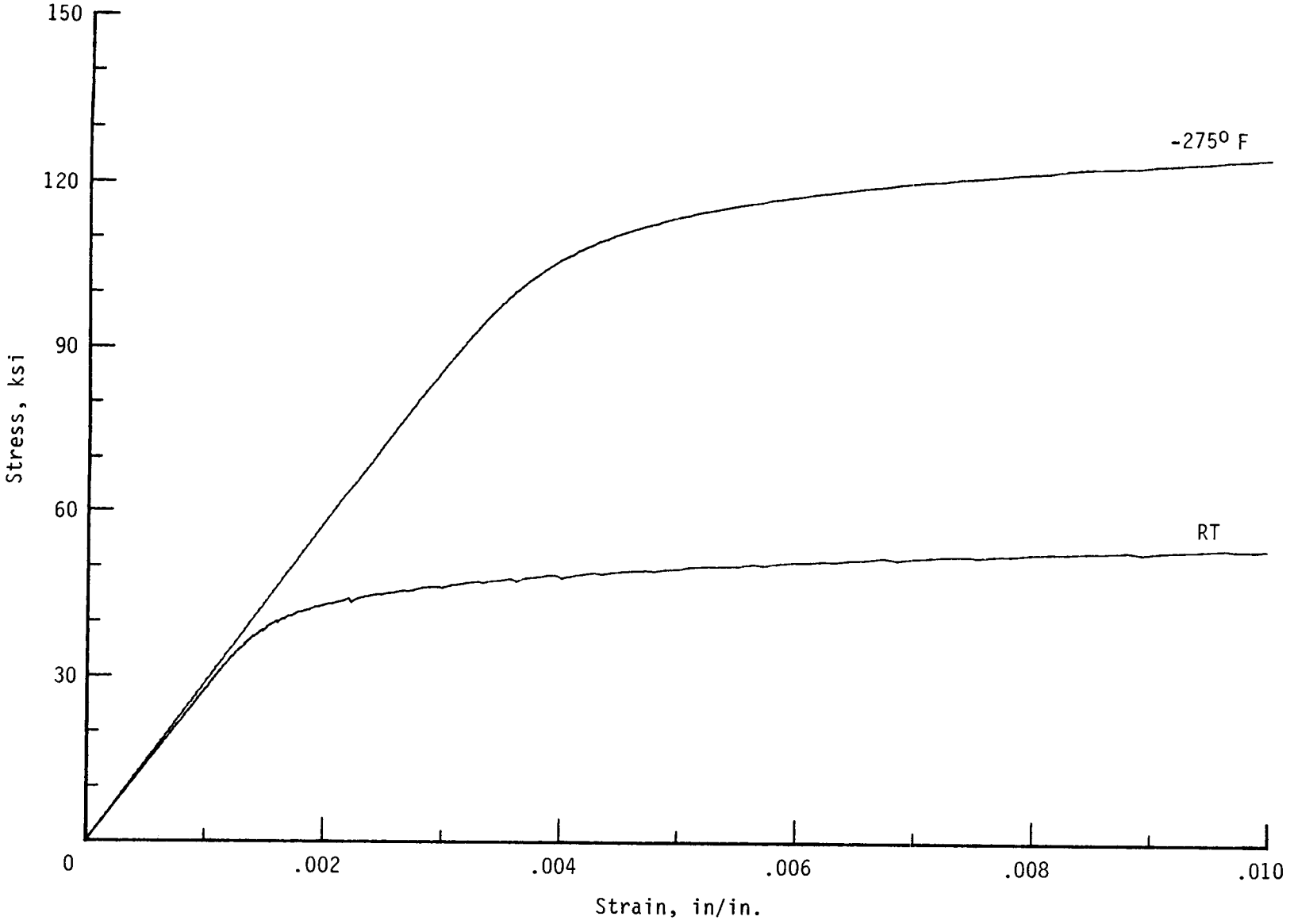

Figure 11.- Typical tensile stress-strain curves for Nitronic 40 specimens at room and cryogenic temperatures.

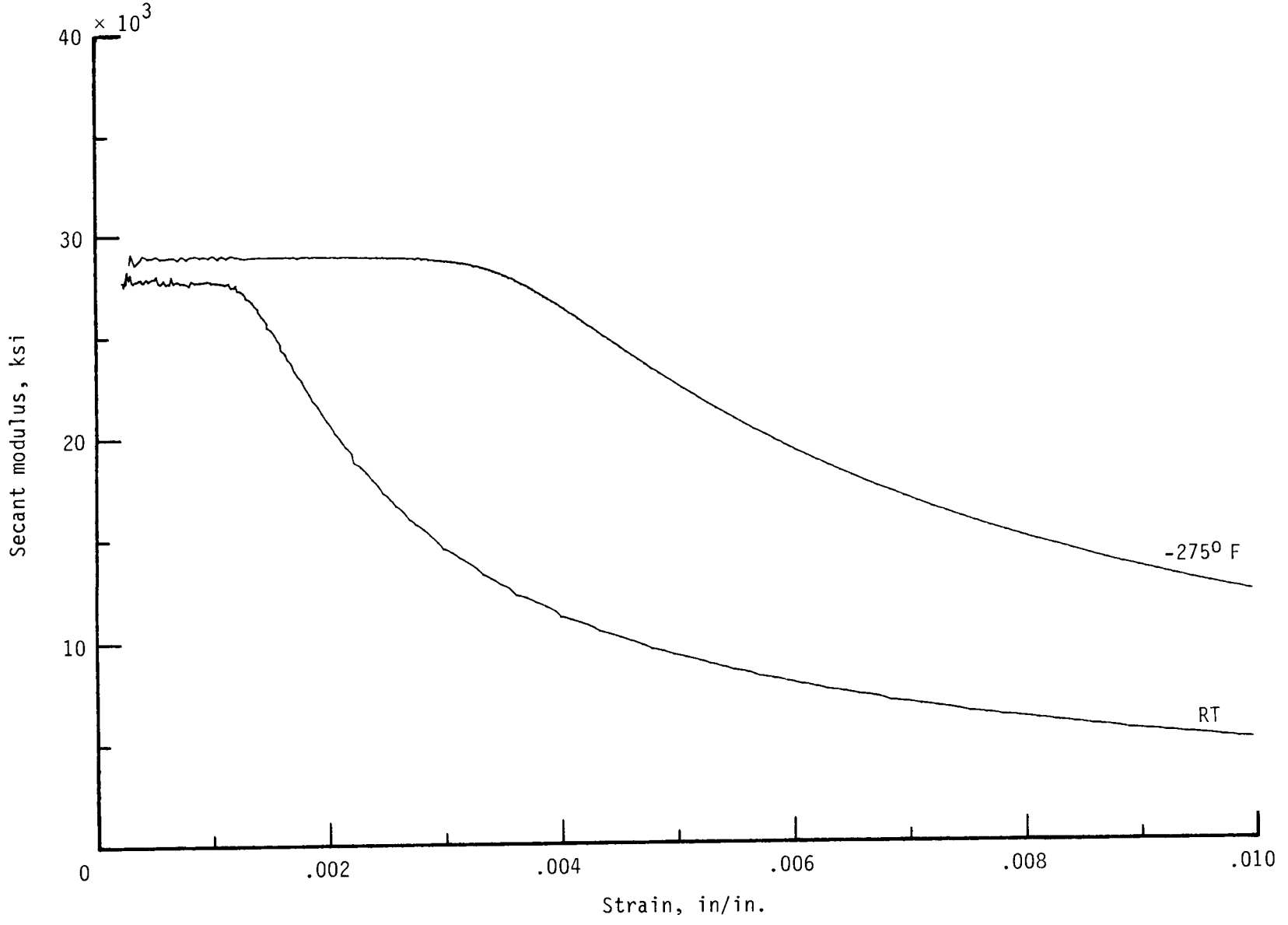

Figure 12.- Typical secant modulus curves for Nitronic 40 at room and cryogenic temperatures.

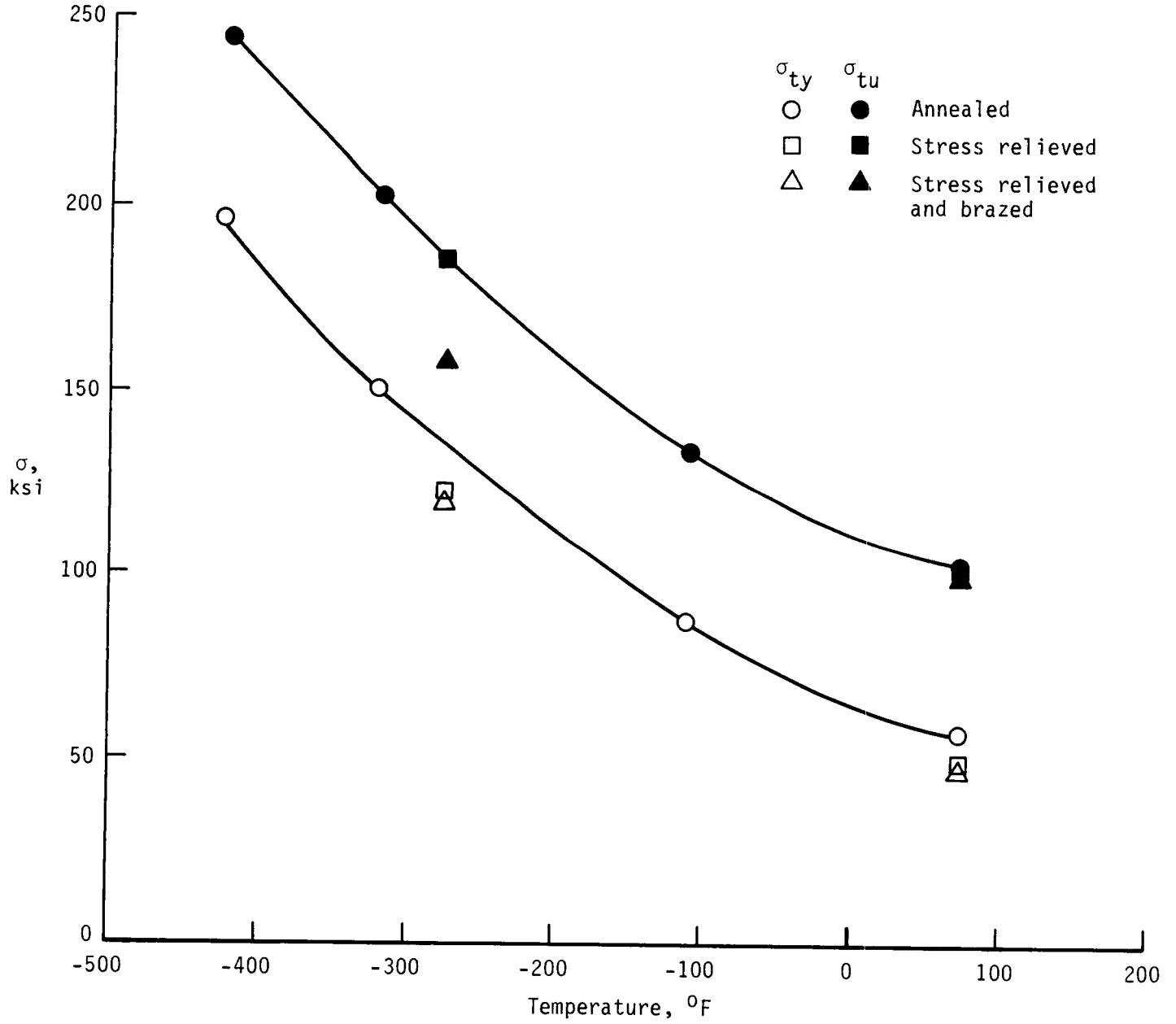

Figure 13.- Tensile property variation with temperature for Nitronic 40.

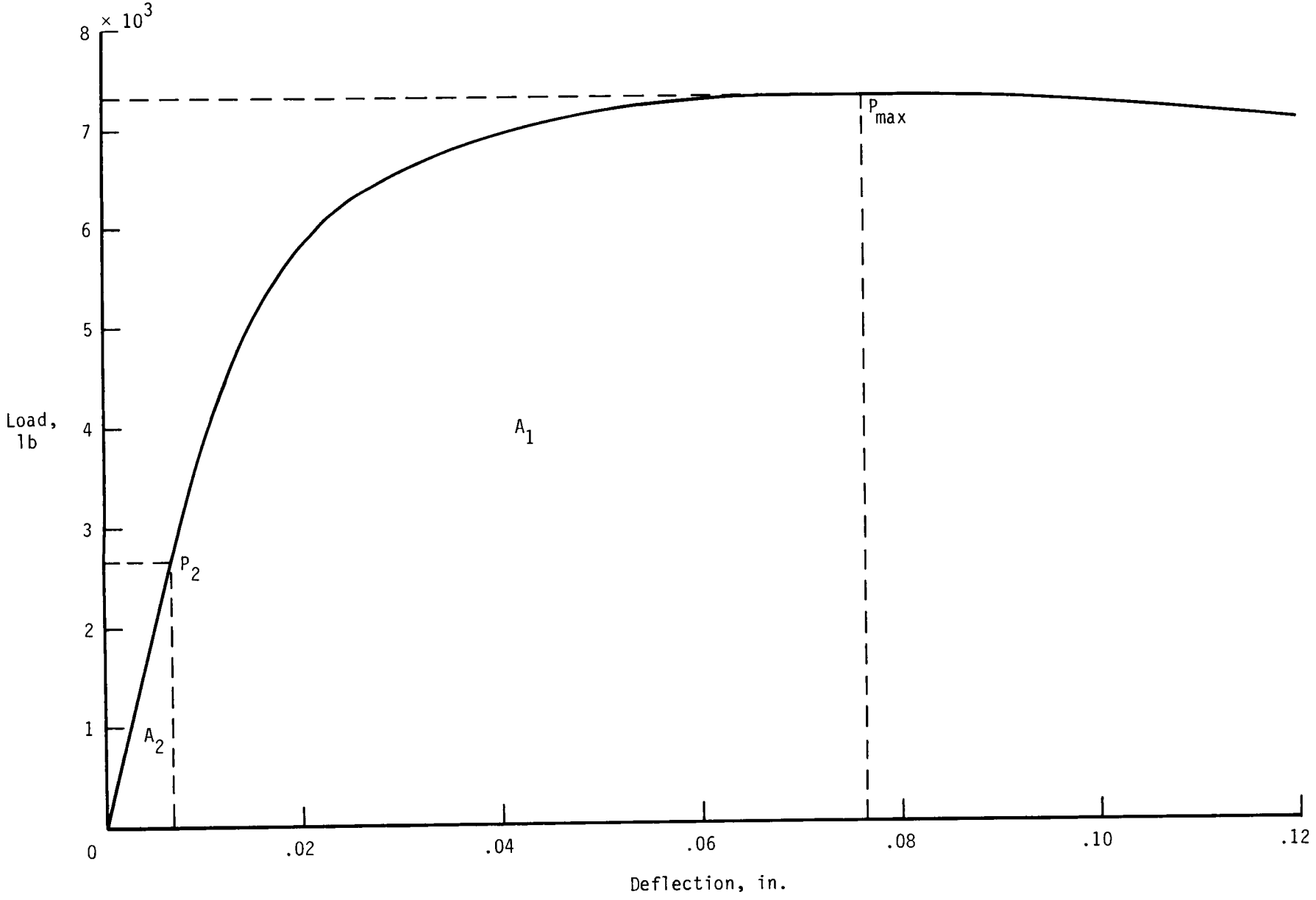

Figure 14.- Load-deflection curve for Nitronic 40 stress-relieved single-edge-notch bend specimen at -275°F.

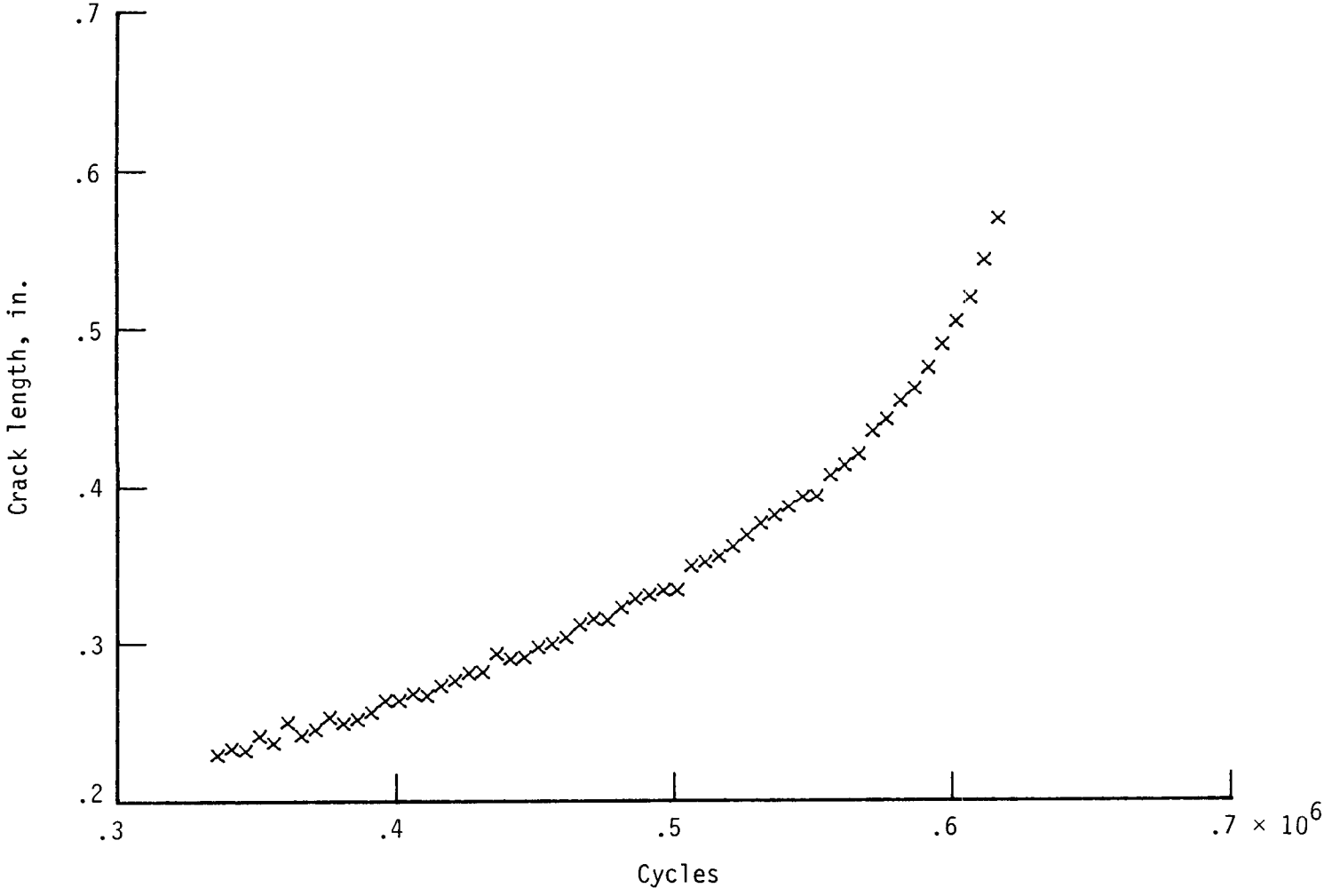

Figure 15.- Fatigue crack growth for annealed Nitronic 40 at -275°F.
R = 0.1; P_{max} = 3000 lb.

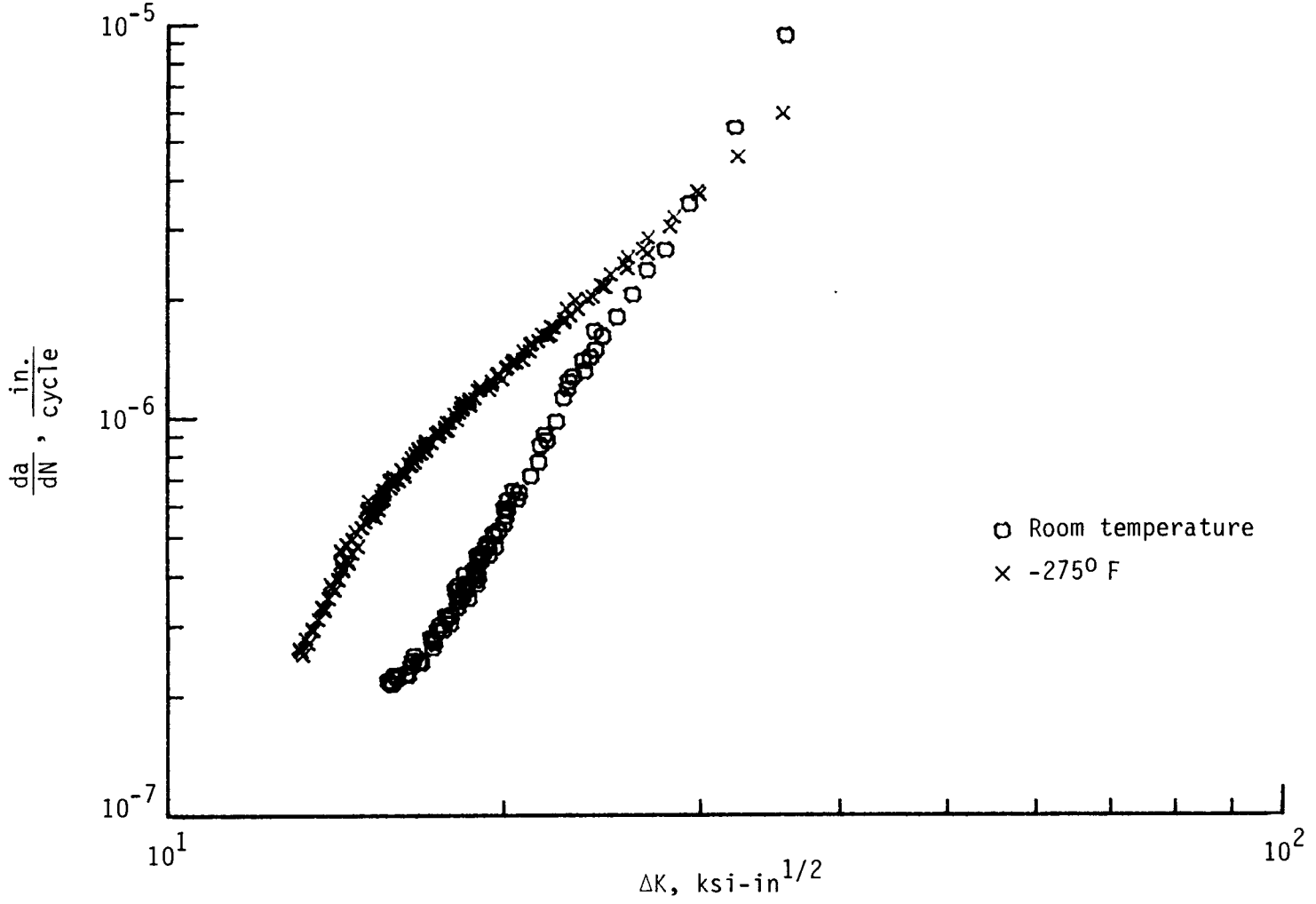

Figure 16.- Fatigue crack growth rates for Nitronic 40 at room and cryogenic temperatures. R = 0.1.

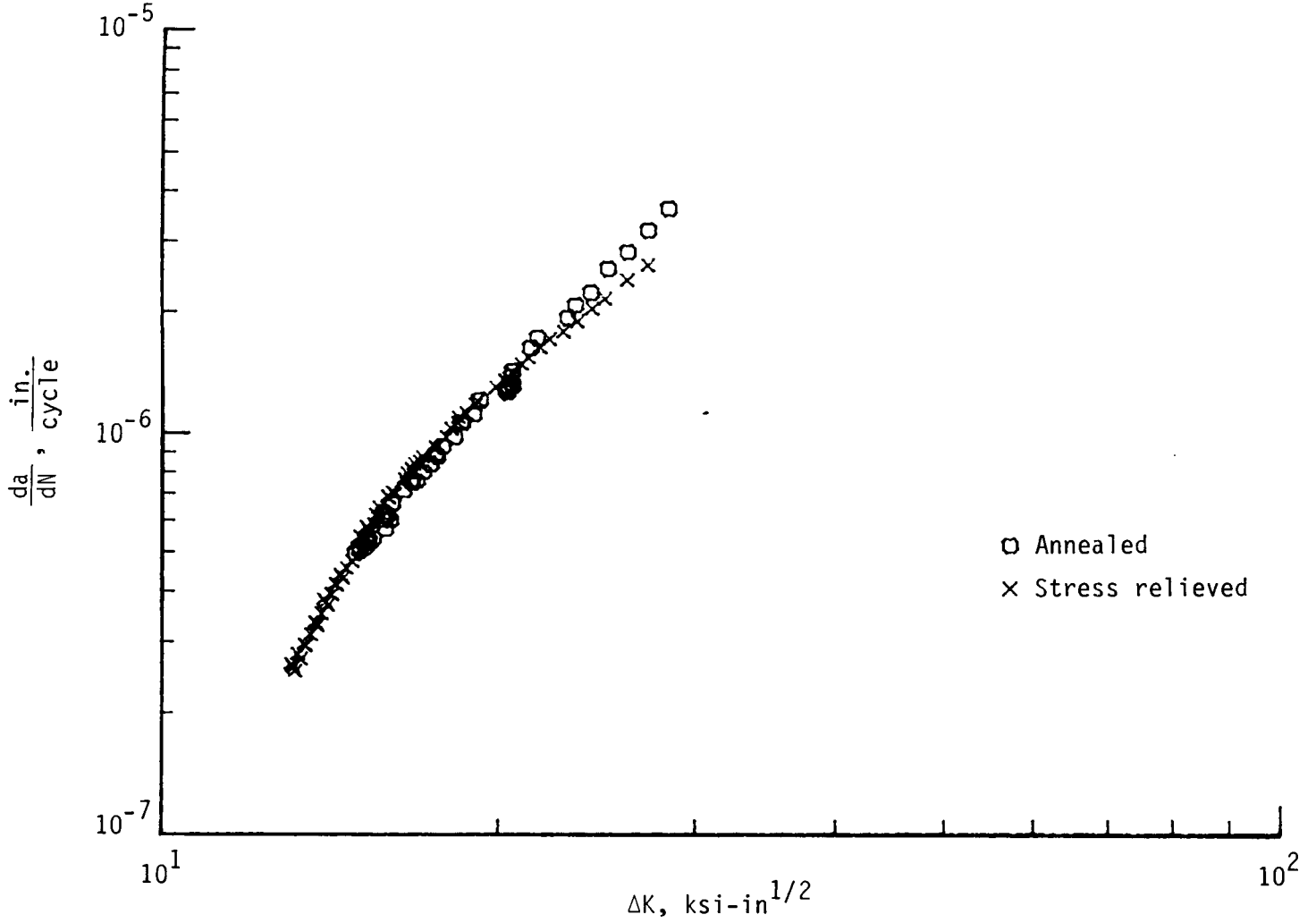

Figure 17.- Effect of material condition on fatigue crack growth rate of Nitronic 40 at -275°F. R = 0.1.

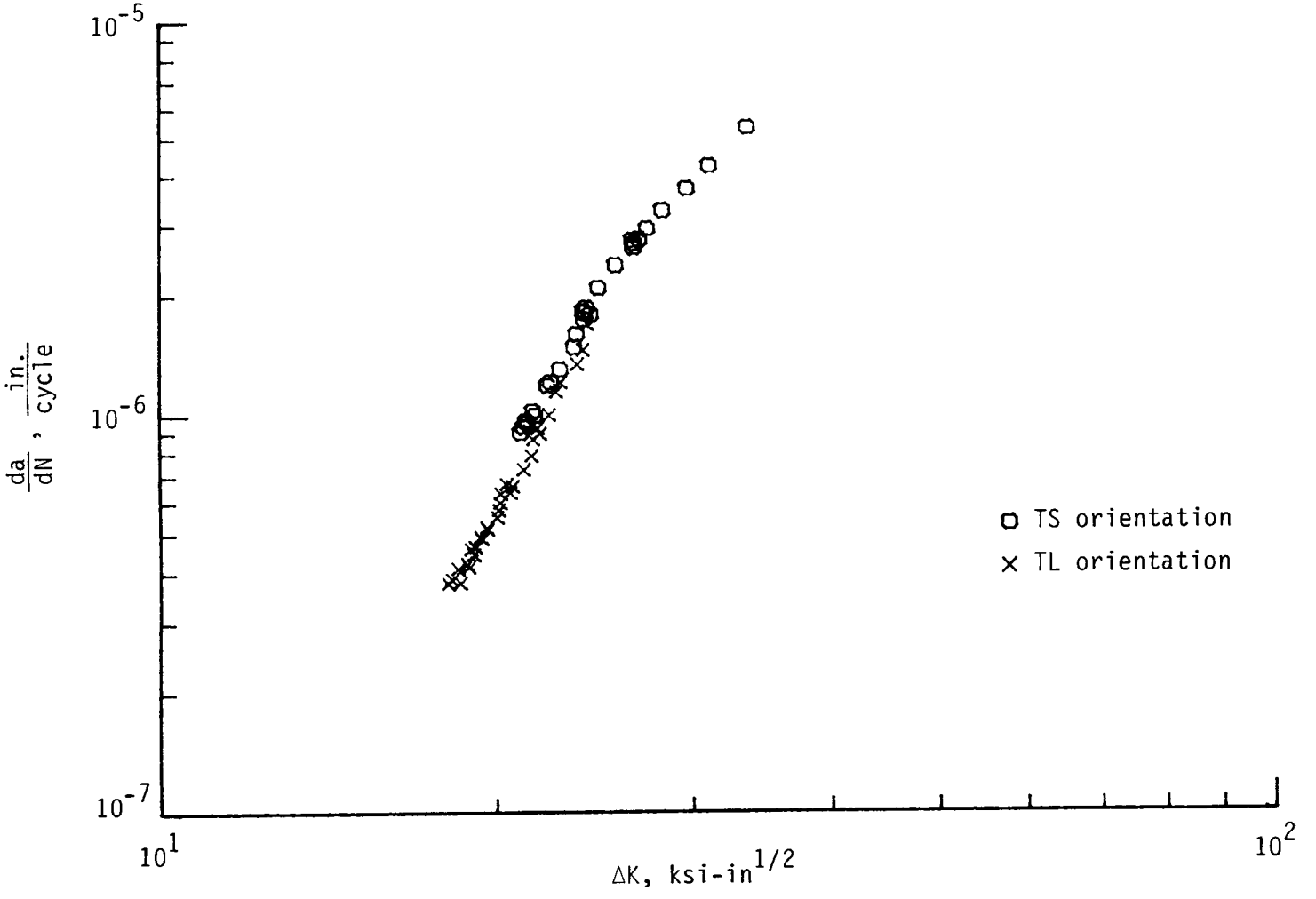

Figure 18.- Effect of specimen orientation on fatigue crack growth rate for Nitronic 40 at room temperature. R = 0.1.

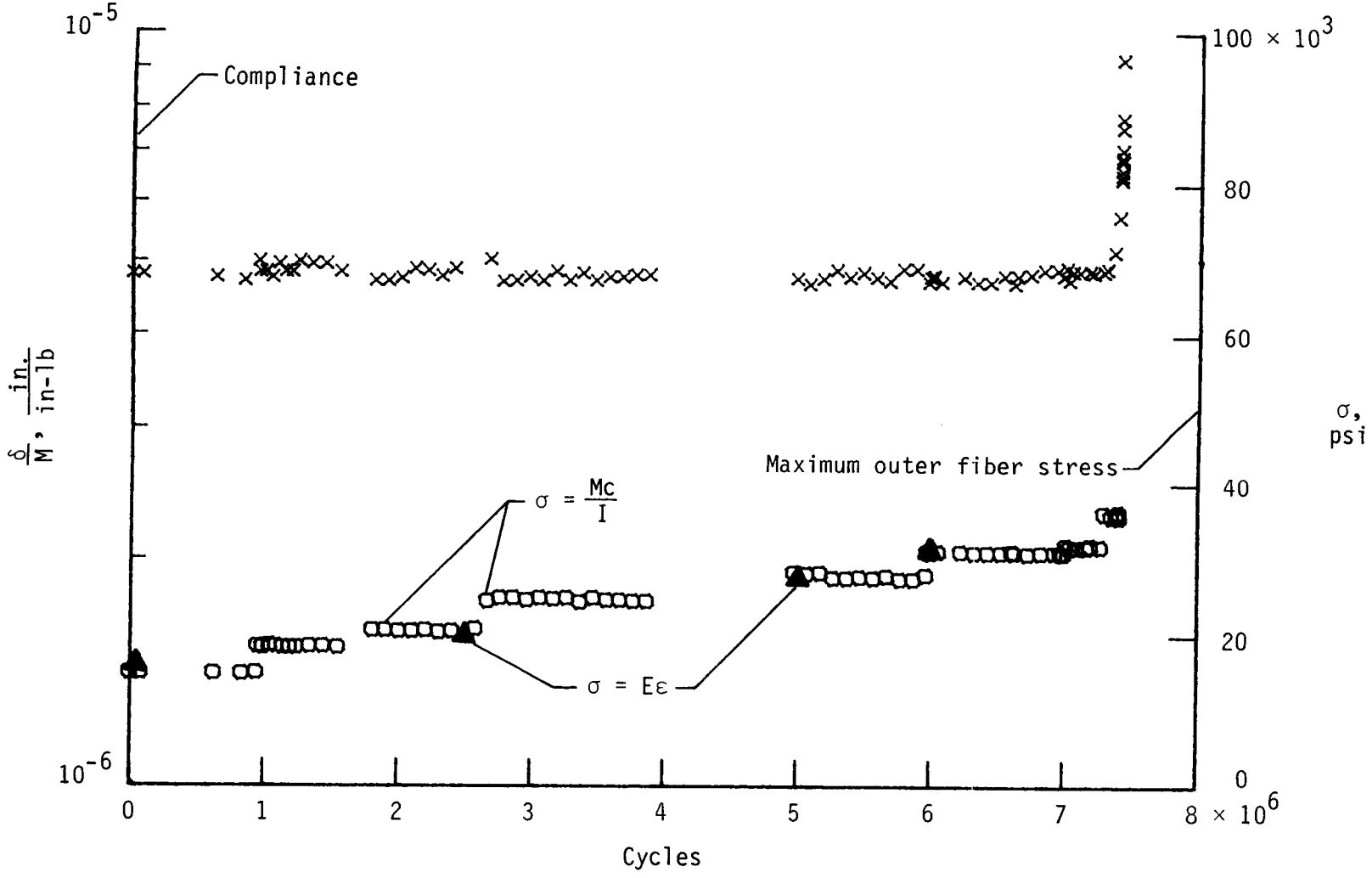

(a) Room temperature; $R = 0.05$; $\sigma_{ty} = 50$ ksi.

Figure 19.- Compliance and stress history for Nitronic 40 wing simulation tests.

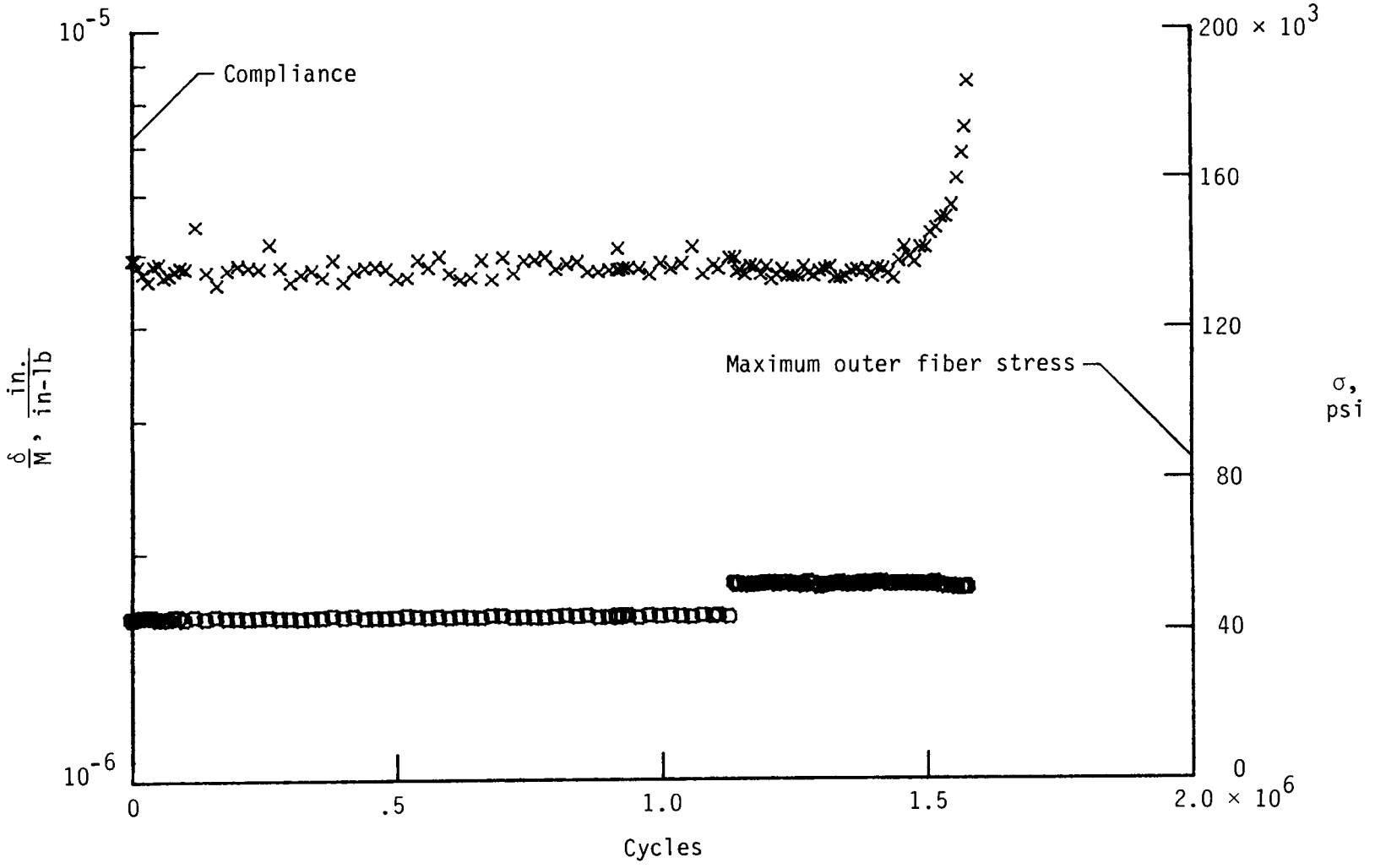

(b) -275°F; R = 0.05; σ_{ty} = 120 ksi.

Figure 19.- Continued.

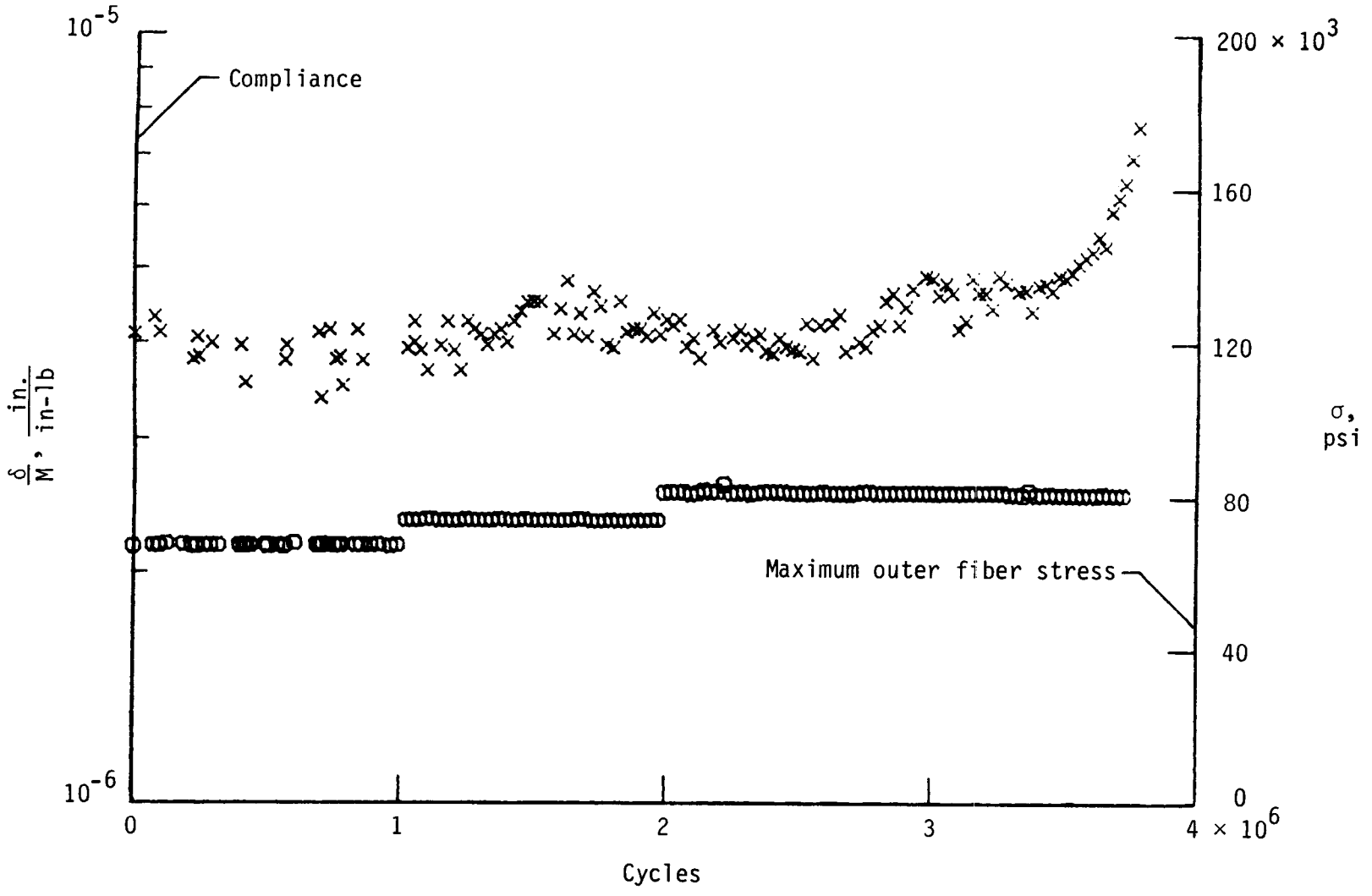

(c) -275°F; R = 0.75; σ_{ty} = 120 ksi.

Figure 19.- Concluded.

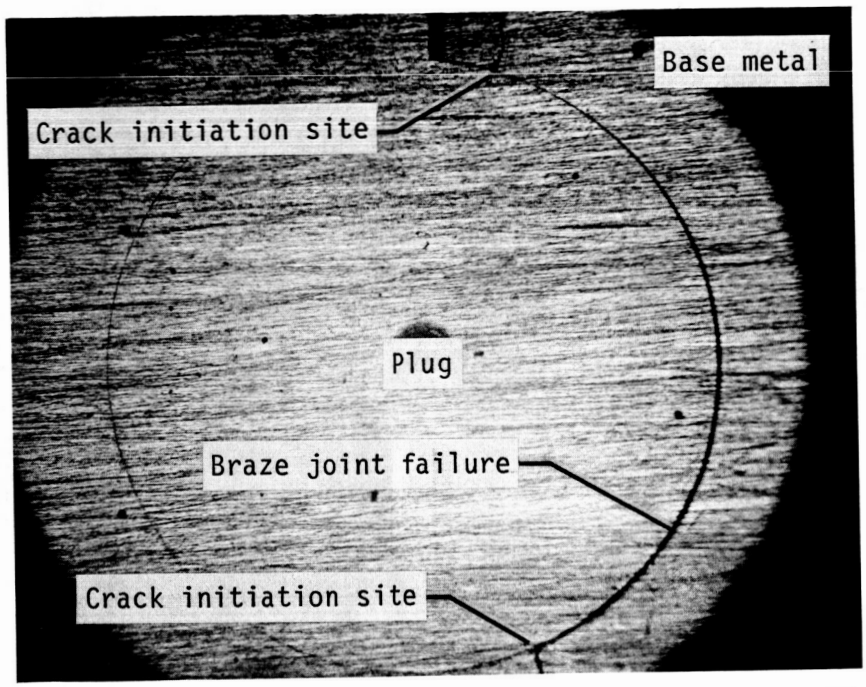

L-84-39

Figure 20.- Fatigue crack initiation sites at brazed plug-base metal interface. (×25)

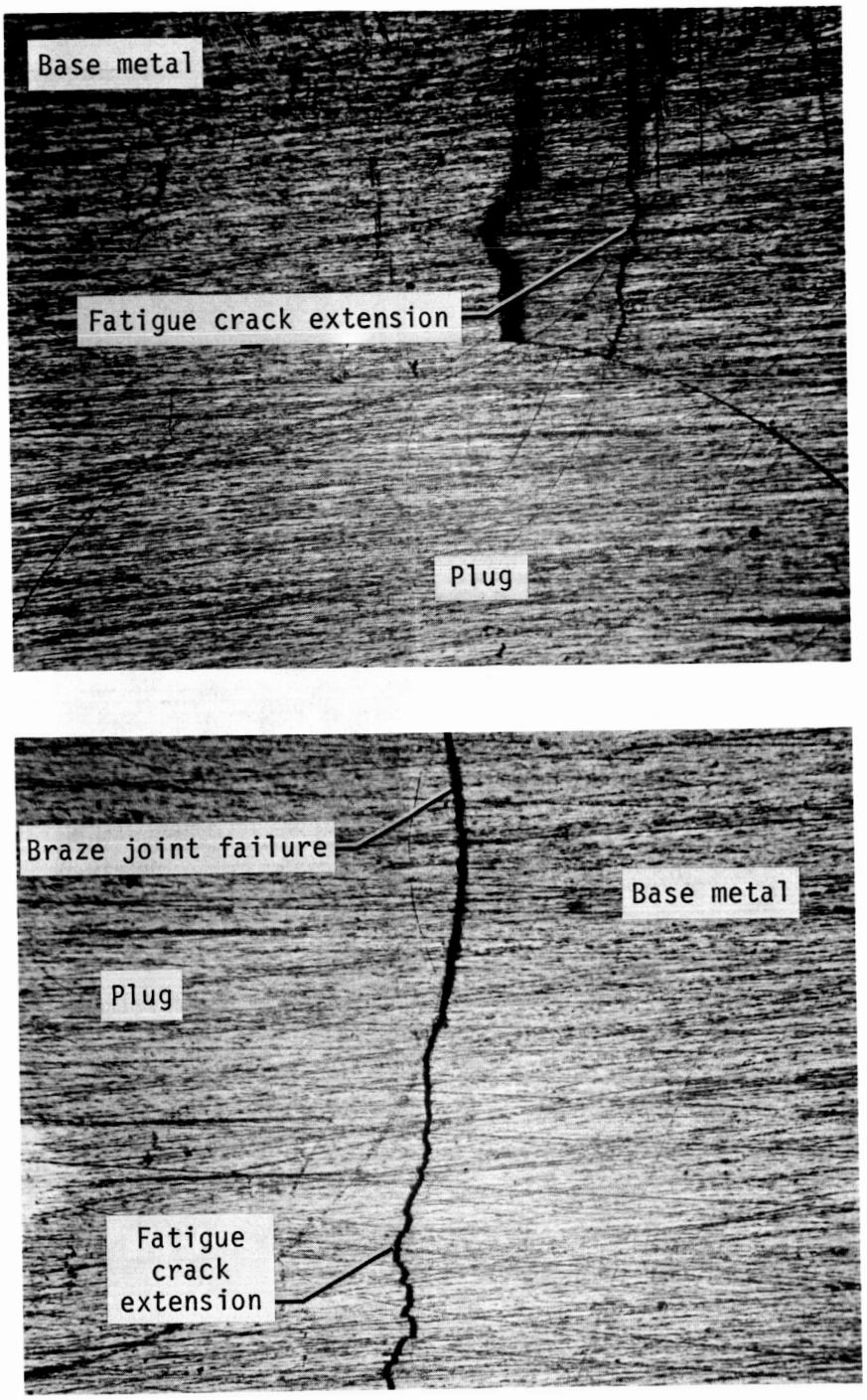

L-84-40

Figure 21.- Typical fatigue crack extension into base metal from initiation sites. (×45)

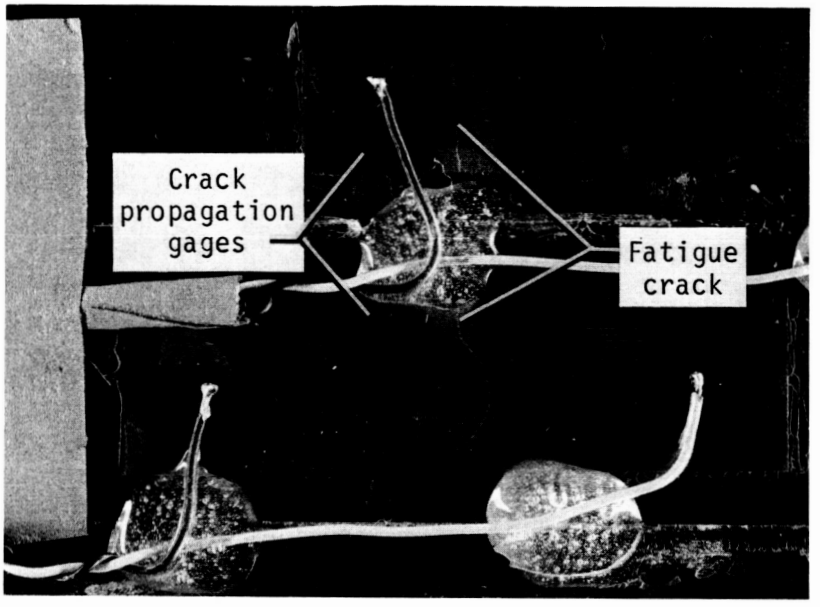

L-84-41

Figure 22.- Fatigue cracking in wing simulation specimen after 3 million cycles at -275°F and R = 0.75. (×3)

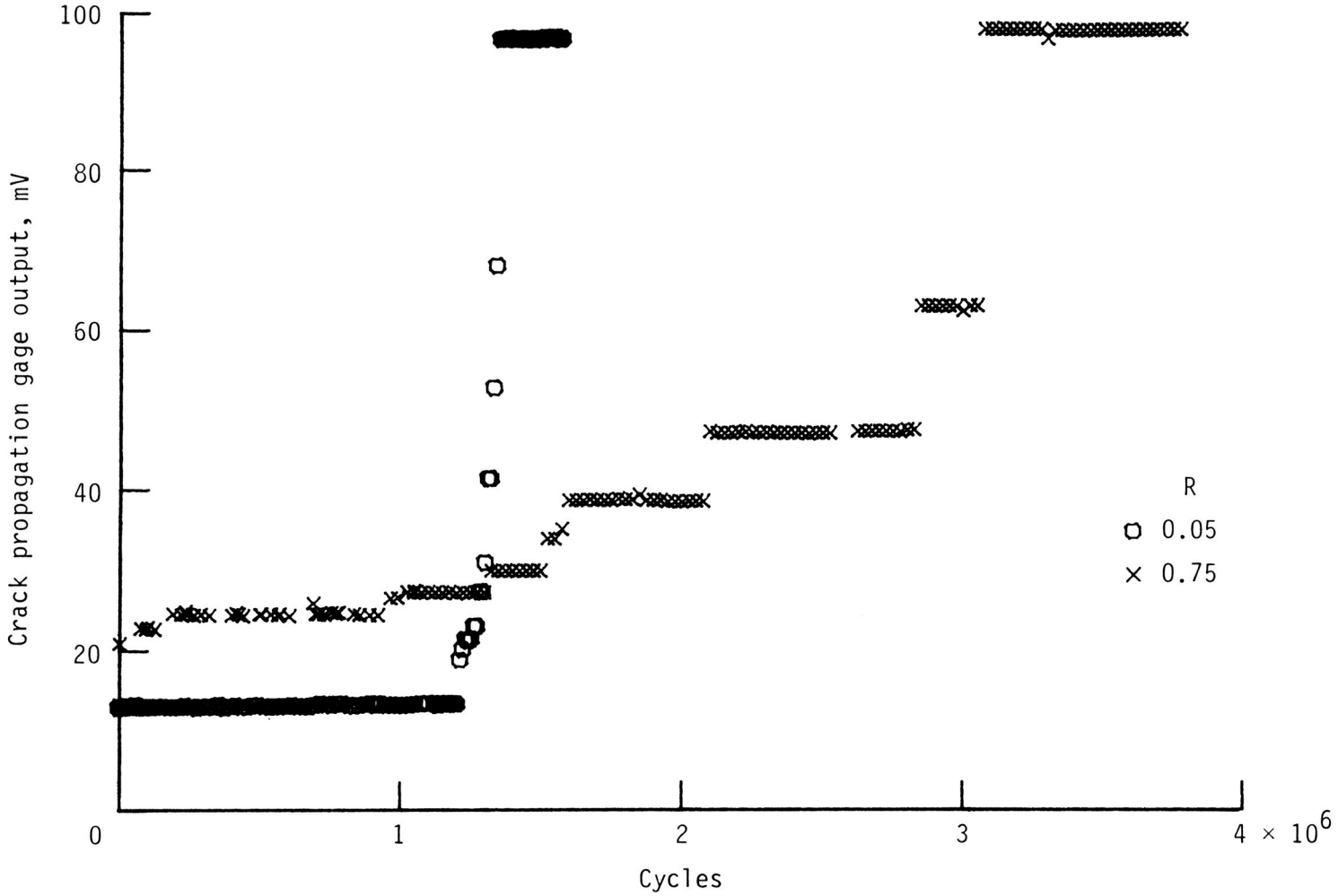

Figure 23.- Fatigue crack growth behavior at different values of R for Nitronic 40 at -275°F.

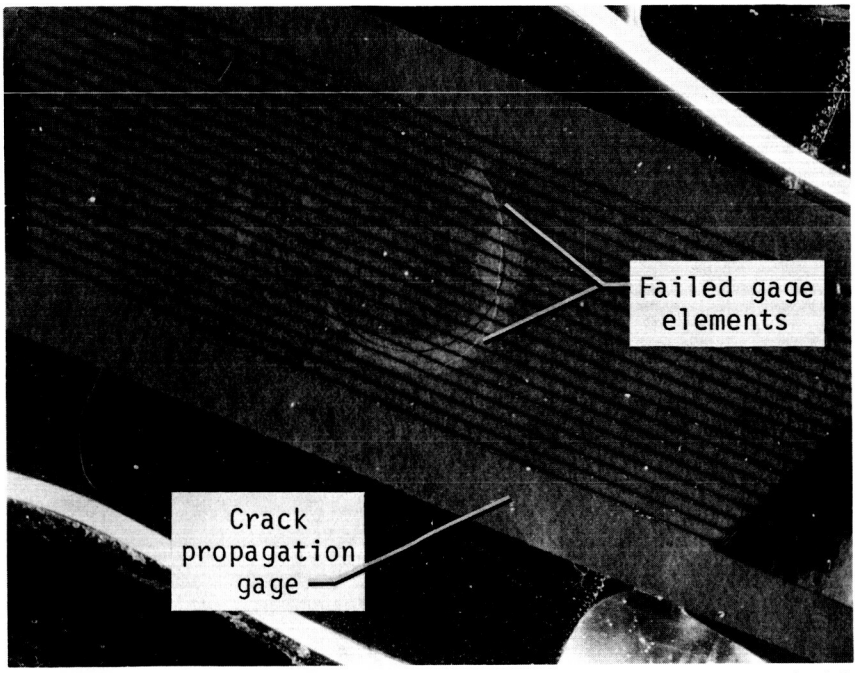

L-84-42

Figure 24.- Crack propagation gage appearance showing gage element failure upon initial loading. (×8)